NUMERICAL MODELING OF THE GROUNDWATER IN THE EAST RIFT ZONE OF KILAUEA VOLCANO, HAWAII

A THESIS SUBMITTED TO THE GRADUATE DIVISION OF THE UNIVERSITY OF HAWAII IN PARTIAL FULFILLMENT OF THE REQUIREMENTS FOR THE DEGREE OF

MASTER OF SCIENCE

IN GEOLOGY AND GEOPHYSICS

AUGUST 1984

By

Jewelle Akie Imada

Thesis Commitee:

Frank L. Peterson, Chairman

David Epp

Clark C. K. Liu

We certify that we have read this thesis and that, in our opinion, it is satisfactory in scope and quality as a thesis for the degree of Master of Science in Geological and Geophysical Sciences.

THESIS COMMITTEE

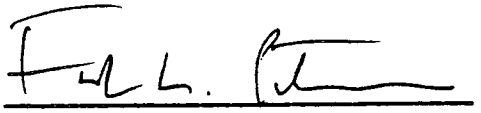

Chairman

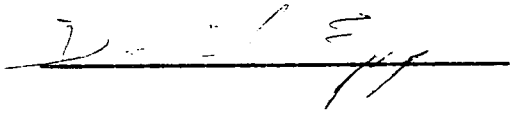

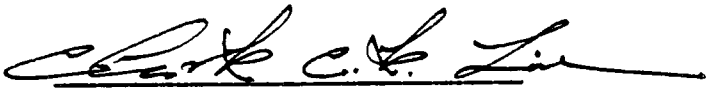

ACKNOWLEDGEMENTS

Although this thesis bears my name it would not have been successfully completed without the help of many people. The author wishes to express sincere appreciation to: the Hawaii Natural Energy Institute (HNEI) for their finacial support which made this project possible, Frank L. Peterson and David Epp for their considerable guidance, Clark C. K. Liu for his advice and assistance in the computer modeling, Pearl Y. Imada for her invaluable help, Donald M. Thomas for insightful comments, my parents for their faith and support and my friends for their encouragement and companionship.

Abstract

The present study was a first attempt to incorporate the effects of groundwater flow, water temperature, and water chemistry in a numerical model of Puna. The calibration of the model identified the east rift zone and temperature to be the most significant factors controlling the hydrology of Puna.

Once the model was calibrated, the effects of seepage of geothermal effluent into the shallow groundwater were examined. The simulations showed that the consequences of the injection of geothermal effluent is a direct function of the salinity of the effluent. The seepage of effluent of very high salinities may cause long term water quality problems. The model was further tested by comparing the results of the simulations with chloride concentrations measured from wells in 1981. The model underestimated the changes in chloride concentration.

TABLE OF CONTENTS

LIST OF TABLES

TABLE

LIST OF ILLUSTRATIONS

FIGURES

LIST OF SYMBOLS

B_{ij}	Coefficient in difference equation
b	Saturated thickness (L)
C	Concentration of the dissolved chemical species (M/L^3)
C'	Concentration of the dissolved chemical species in a sink or source fluid
D_{ij}	Dispersion coefficient (L^2/t)
D_L	Longitudinal dispersion coefficient (L^2/t)
D_T	Transverse dispersion coefficient (L^2/t)
E	Coefficient of difference equation
E_c, E_r	Coefficients in equations defining IADI
F	Flux of fluid movement (M/tL^2)
F_{ij}	Coefficient in differenc equation
g	Acceleration due to gravity (L/t^2)
H_{ij}	Coefficient in difference equation
h	Hydraulic head (L)
h_f	Hydraulic head in the freshwater measured above sea level (L)
h_s	Hydraulic head in the saltwater measured below sea level (L)
i	Index in the y direction
j	Index in the x direction
K_{ij}	Hydraulic conductivity tensor (L/t)
k	Time index
k_{ij}	Intrinsic permeability tensor (L^2)
$k_{non-rift}$	Assigned intrinsic permeability of non-rift area (L^2)
k_{rift}	Assigned intrinsic permeability of rift area (L^2)

ℓ	Iteration parameter index
M_ℓ	Iteration parameter
N_x	Number of nodes in the x direction
N_y	Number of nodes in the y direction
n	Iteration index
P	Pressure (M/t^2L)
Q	Discharge of water (L^3/t)
Q	Known term in difference equation
Q_c, Q_r	Known terms in equation defining IADI
Q_w	Well discharge (L^3/t)
q	Specific discharge (L/t)
q_{re}	Diffuse recharge per unit area (L/t)
Sy	Specific yield (dimensionless)
T	Temperature
t	Time dimension
W(x,y,t)	Volume flux per unit area (L/t)
$\|V\|$	Magnitude of velocity vector (L/t)
V_i	Average velocity (L/t)
V_m	Component of velocity in the m direction (L/t)
V_n	Component of velocity in the ndirection
x_i, x_j	Cartesian coordinates
x, y, z	Cartesian coordinates
z	Elevation above some datum(L)
z	Interface location below sea level (L)
	Porosity (dimensionless)

α	Dispersivity (L)
α_L	Longitudinal dispersivity (L)
α_T	Transverse dispersivity (L)
β	Assigned dispersivity (L)
γ	Specific weight of water ($M/L^2 t$)
Δt	Time increment
Δx	Space increment in the x direction (L)
Δy	Space increment in the y direction (L)
ε	Effective porosity (dimensionless)
μ	Dynamic viscosity (M/Lt)
ρ	Density of water (M/L^3)
ρ_s	Saltwater density (M/L^3)
ρ_f	Freshwater density (M/L^3)
∇	Vector operator

CHAPTER I

INTRODUCTION

Background

There is considerable interest in the geothermal potential of the Puna district on the Island of Hawaii. Although extensive studies have been undertaken to assess this potential, relatively little is known about the hydrology of Puna. Examination of the interrelationships between groundwater flow, water temperature, and water chemistry is necessary to accurately describe the groundwater system. A better understanding of the hydrology is essential to fully utilize the geothermal resources of the area. It is in response to these needs that the present study was undertaken.

The area under investigation is situated on the east rift zone of Kilauea (Figure 1). It includes a 240 square kilometer area that ranges in altitude from sea level to about 122 meters (400 ft) above sea level.

Geothermal Development

Geothermal development in Puna began in the early 1960's with the drilling of four exploration wells. The wells were relatively shallow, between 100 and 200 meters. Although temperatures between 43 to 93 °C were measured in the wells, the amount of steam produced by these wells was not sufficient for geothermal production (Druecker and Fan, 1976, Kroopnick et al., 1980).

In 1976, HGP-A was drilled to a depth of 1966 m (6450 ft) or a depth of 1768 m below sea level. It was the deepest well in the area and a temperature of 358 °C was measured at the bottom, making it also the hottest well in Puna.

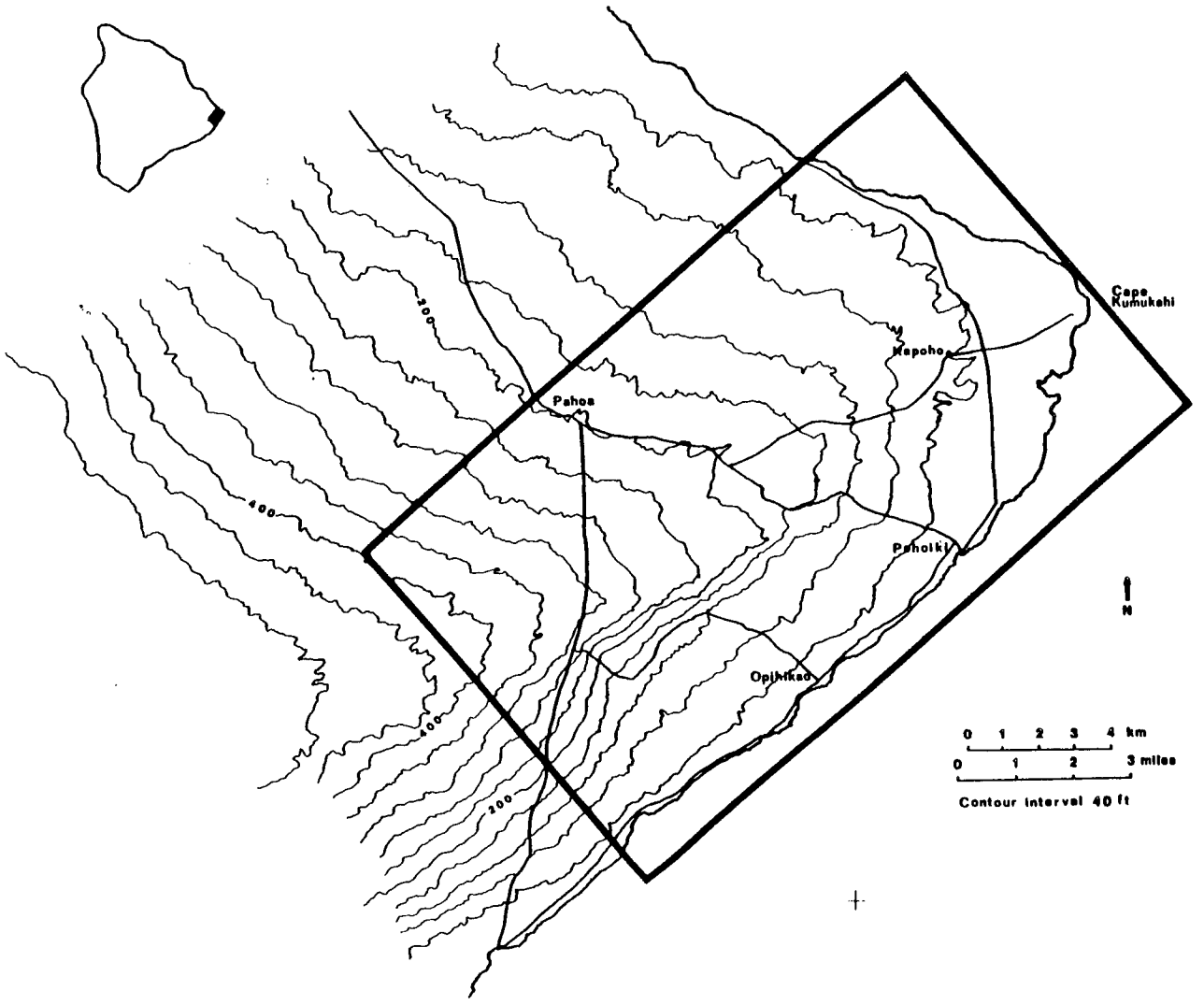

Figure 1. Study Area Location Map

Presently HGP-A is providing steam to a three megawatt generator and is estimated to be capable of producing approximately 50,000 kg/hr of geothermal fluid (43% steam, 57% brine) at well head pressures of 1172 kPa (Thomas and Sakai, 1983).

Between 1980 and 1982, four private geothermal wells have been drilled (Figure 2 and Table 1). All the wells are deep, greater than 2000 m and report bottom temperatures in excess of 200 ° C. Further geothermal exploration is expected to continue through 1990.

Table 1

Information on Thermal Springs and Wells*

USGS Number	Name	Depth (m)	Termperature (°C)	Comments
2487-01	Keauohana-1	240.6	24	
2487-02	Keauohana-2	240.6	24	
2685-01	Ashida 1	>2000	>200	Proprietary
2686-01	GTW-1	169.5	102	
2783-01	Malama-ki	95.7	55	
2881-01	Pohiki	42	38	
2883-01	HGP-A	1967.5	358	
2883- x	Lanipuna 1	>2000	>200	Proprietary
2883- x	Kapoho State 1	2187	>200	Proprietary
2883- x	Kapoho State 2	>2000	>200	Proprietary
2982-01	GTW-3	210.3	93	
3081-01	Kapoho Test	131	101	
3081-02	GTW-4	88.4	43	
	Allison Spring		31	
	Opihikao Spring		38	
	Issac Hale Spring		36	

*from Geothermal Resources of Hawaii, 1983

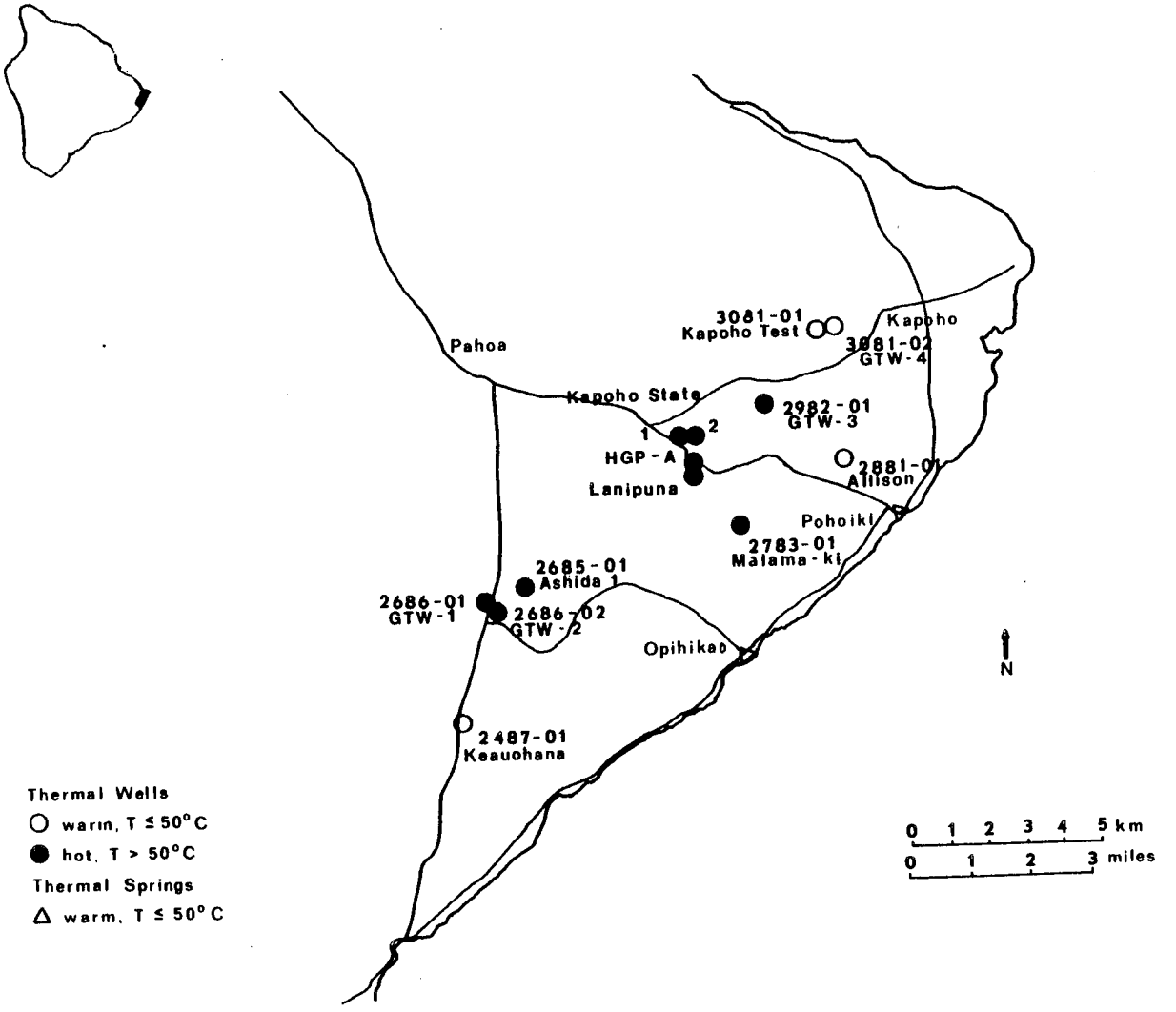

Figure 2. Locations of Thermal Wells and Springs (from Geothermal Resources of Hawaii, 1983)

Objectives

The major objectives of this study are twofold: first, to gain insight into the existing condition of groundwater hydrology in the geothermal area of Puna, and secondly, to determine the effects of the disposal of geothermal effluent on the groundwater.

The initial phase of the study concentrates on the collection of available information on the hydrology, geology, meteorology, geochemistry and temperature of groundwater in the area.

The next phase consists of the development of a numerical model which simulates the hydrologic conditions of Puna. The model considers the interrelationships between groundwater flow, water temperature, and water chemistry. The model is calibrated and verified using data from water wells and test holes. A water budget is computed using a mass balance approach, thus providing an estimate of water quantity which is constrained by available geohydrological data.

Once calibrated, the model is used to investigate the effects of geothermal effluent on the shallow groundwater. The distribution of geothermal effluent over time is evaluated.

The results of this study provide a means to examine long term effects of future geothermal development on the groundwater resources in the area and give some insights into the mechanisms controlling the chemistry of the Puna wells.

CHAPTER II

GEOHYDROLOGY

Meteorlogy

The median rainfall in Puna is about 250 cm/yr (Figure 3). The north central areas have a high rainfall of about 350 cm/yr while the southeastern coast is drier with approximately 200 cm of rainfall per year. Variations in both monthly and annual rainfall is large. Although monthly rainfall variation indicates no definite wet or dry season, June and September are relatively dry and November and December are relatively wet.

Since there are no surface waters in Puna, an estimate of the evaporation would enable a direct calculation of the amount of recharge to the aquifer from the precipitation. Unfortunately, there are no pan evaporation stations in the area. Imada (1982) used the relationship between evaporation and net solar radiation to calculate the average annual evaporation for the raingage stations in the area.

Geology and Geophysics

The island of Hawaii is composed of five major shield volcanoes: Kohala, Mauna Kea, Hualalai, Mauna Loa, and Kilauea. Only Mauna Loa and Kilauea are still active.

Lava found in Puna is from both Mauna Loa and Kilauea. The Kau and Kahuku volcanic series of Mauna Loa have been overlain by the more recent Puna volcanic series of Kilauea (Figure 4). The stratigraphic relationships of the volcanic series and their water bearing properties are listed in Tables 2 and 3.

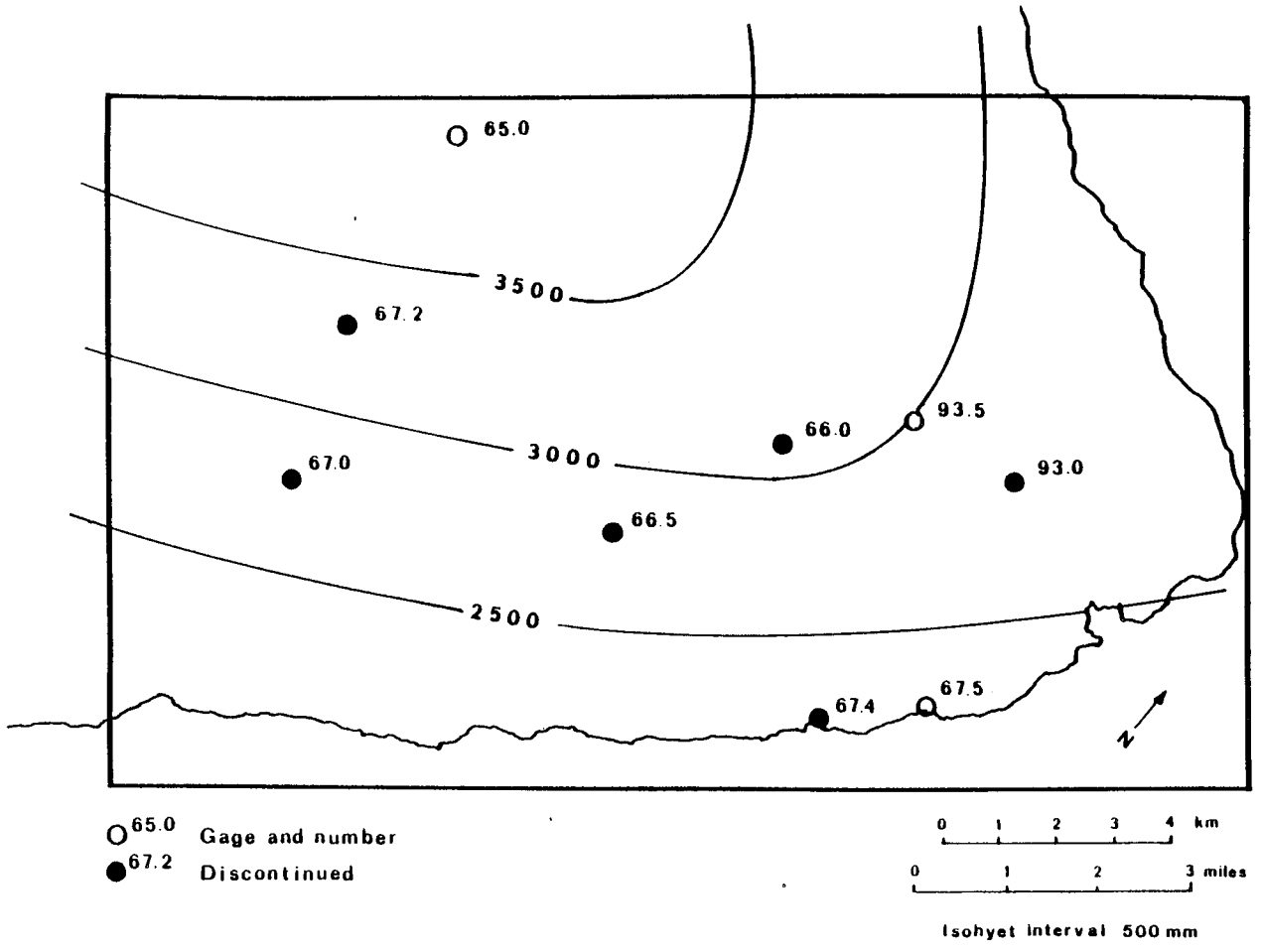

Figure 3. Annual Median Rainfall (DOWALD, 1982)

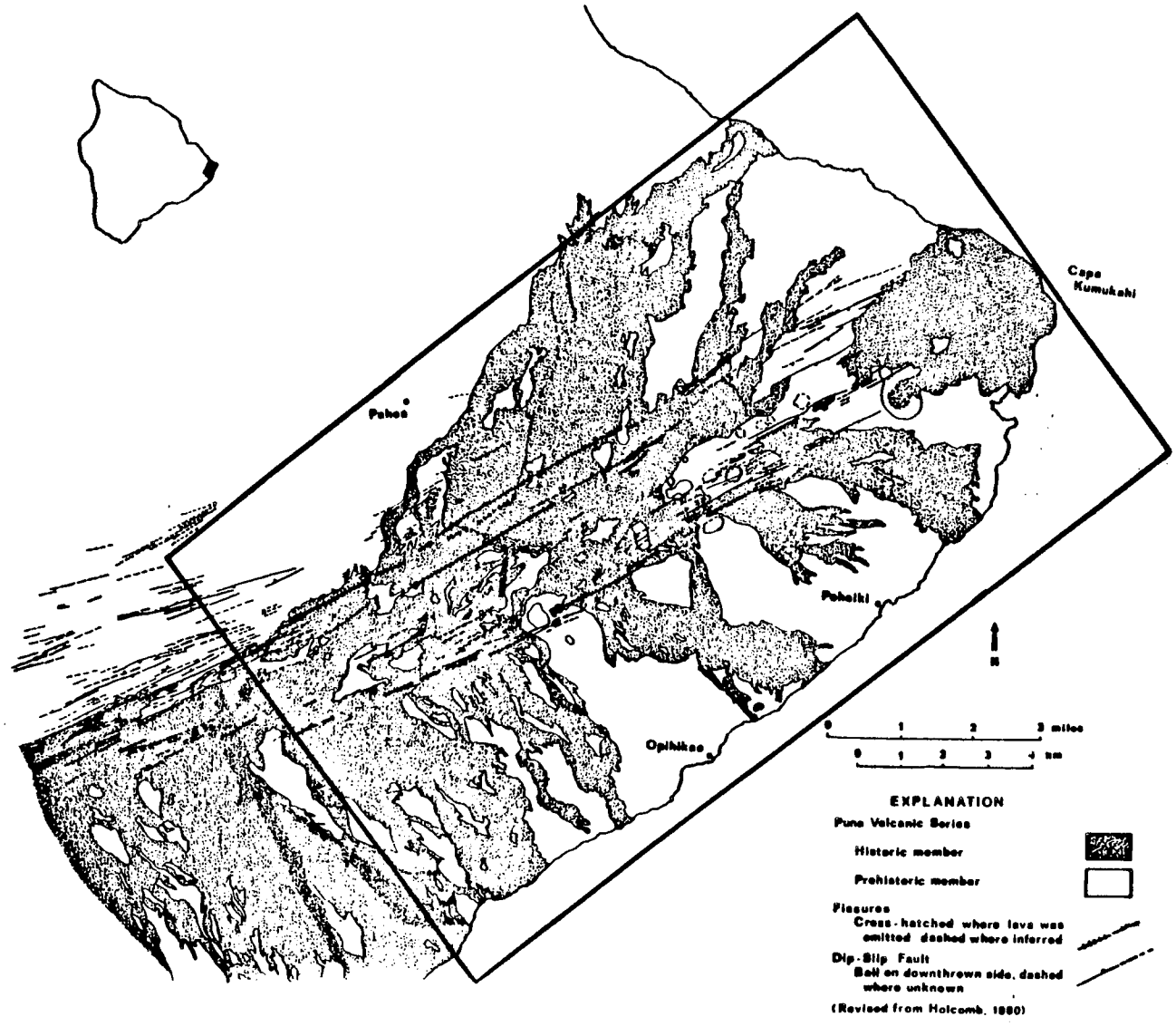

Figure 4. Geologic Map (Revised from Holcomb, 1980)

Table 2

Rock Sequence for Mauna Loa*

Age	Rock Assemblages	General Character	Water Bearing Properties
Recent	Lava flows and cones; historic member of the Kau Volcanic Series.	Aa and pahoehoe basalt flows, cinder spatter cones.	Extremely permeable, but rock mostly above the water table.
	Unconsolidated deposits.	Small amounts of beach sand and alluvium.	Highly permeable but dry, except at the shore where water is brackish.
	Prehistoric member of Kau Volcanic Series.	Aa and Pahoehoe basalt forming a nearly complete veneer over Mauna Loa; cinder and spatter cones, littoral cones and some ash deposits.	Extremely permeable. Large springs discharge at shore from these rocks. In wet upland areas, lava may contain water perched on ash beds
Pleistocene	Pahala Ash	Fiable ash composed chiefly of dust to sand-sized particles of palagonitized shards of volcanic glass and pumice.	Less permeable than lava flows, perches water overlying lava flows in some upland wet above Hilo, forming high level springs.
	Kahuku	Aa and pahoehoe basalt flows; cinder cones, littoral cones.	Highly permeable. Water brackish near coasts but fresh near sea level farther inland.
		Erosional unconformity	
Pliocene	Ninole Volcanic Series	Aa and pahoehoe basalt flows.	Highly permeable. Contain freshwater at sea level.

* From Davis and Yamanaga, 1968

Table 3

Rock Sequence of Kilauea Volcano*

Age	Rock Assemblages	General Character	Water Bearing Properties
Recent	Lava flows, cones, and explosion deposits historic member of Puna Volcanic Series.	Aa and pahoehoe flows cinder and splatter cones, littoral cones.	Extremely permeable, but above the water table except near the shore where water is commonly brackish.
	Unconsolidated windblown sand and beach deposits.	Composed of sand from ash and basaltic sand in beach deposits.	Contain water only at shore where water is brackish.
	Prehistoric member of the Puna Volcanic Series.	Aa and pahoehoe basalt flows; cinder and spatter cones, littoral cones and ash beds.	Extremely permeable except for ash deposits, which have relatively low low permeablity.
Pleistocene	Pahala Ash	Chiefly palagonitized basaltic pumice fragments and shards.	Low permeability.
Pleistocene and Pliocene (?)	Hilina Volcanic Series	Aa and pahoehoe basal flows.	Highly permeable.

*From Davis and Yamanaga, 1968.

The major structural feature in the area is Kilauea's east rift zone. The rift zone is characterized on the surface by numerous fissures, cones, and pit craters. The eruptive vents indicate that the rift zone is approximately 3 km wide at the surface and may be wider at lower depths (Furumoto et al., 1977). Geophysical studies indicate the existence of a dike complex at a depth of 2.3 km, spanning 12-17 km (Broyles et al., 1979). By analogy with the Koolaus on Oahu, Furumoto et al. (1977) estimated that the dense dike rocks comprise 25-50% of the total rocks within the rift zone. The thin, nearly-vertical dikes lie parallel to the rift zone, intruding into permeable basalt lava flows and dividing the lava flows into separate compartments.

Near the surface, the lava flows are highly vesicular. Pahoehoe flows, containing small and some large unfilled lava tubes, interflow layers, aa clinker zones, and joints, contribute to the high permeability of the surface layers. Thin pyroclastic ash layers a few centimeters to a meter thick, present in some areas, may retard flow. With depth, secondary minerals fill voids in the clinker and interflow layers, thus reducing the porosity and permeability. At approximately 610 meters (2000 ft) below sea level, submarine volcanics appear (Palmiter, 1966). Lava which has erupted below sea level becomes less and less vesicular with increasing water depth until about 1830 m where vesicles essentially disappear. These submarine lava flows are composed of dense pillow lavas and hyaloclastites which causes very low permeabilities. What permeability exists results from fractures in the rift zone (Macdonald, 1977).

The cores taken from HGP-A confirm this change in permeabilities. The surface lavas are unaltered and highly permeable. The uppermost

hydrothermally altered layer occurs between 675 m and 1300 m, where vesicles are partially filled with secondary minerals. This zone is characterized by montmorillonite with minor amounts of calcite quartz, and chlorite. A relatively impermeable layer between 1350 and 1959 m is thought to be the caprock of the geothermal reservoir. In this layer, all of the vesicles have been filled, with chlorite as the predominant mineral. The geothermal reservoir lies below 1959 m, where vesicles are only partially filled, making the rock moderately permeable (Stone, 1977).

An old inactive rift zone of Mauna Loa is thought to underlie the Kilauea lavas in eastern Puna. This may extend the dike complex to a considerable depth (Macdonald, 1977). Moreover, the contact between Kilauea and Mauna Loa lavas may also affect the hydrology. Along this contact, approximately 35 kilometers west of Cape Kumukahi, Kilauea overlaps several meters of relatively impermeable ash which may continue to or beyond Cape Kumukahi at some depth below sea level (Stearns and Macdonald, 1946). If present, the ash layer may form an impermeable cap to groundwater flow (Furumoto et al., 1977). The buttressing of Kilauea against Mauna Loa appears to have an effect on the structure and hydrology of the east rift zone. The slope of Mauna Loa and the pre-Kilauea seafloor are thought to intersect just under HGP-A (Epp et al., 1983). West of this intersection, Kilauea is constrained to expand only to the south, while east of the intersection, the rift can grow in to the north as well. Since the number of dikes decrease with distance from the summit reservior, the reduction of stress resulting from buttressing against Mauna Loa may allow for higher permeabilities.

More detailed accounts of the geology of Puna are given by Stearns and Macdonald (1946), Furumoto et al. (1977), and Macdonald et al. (1983).

Furumoto et al. (1977) summarize the geophysical surveys of Puna conducted as part of the Hawaii Geothermal Project. Seismic studies by Suyenaga et al. (1978) indicate that there are three major seismic velocity layers in the area. The surface layer, consisting of inter-layered pahoehoe and aa lava flows with large voids, has low but variable velocities between 0.8 to 1.6 km/sec. The next layer, indicated by an increase in velocities (2.5-3.0 km/sec) is thought to be caused by water saturating the porous basalt occurs near sea level. The upper boundary of the third layer is located at depths between two and five kilometers and has high velocities (5 km/sec) consistent with a dike complex.

Geoelectrical studies indicate that water with temperatures as high as 200 °C exist and may extend to depths of two kilometers (Keller et al., 1977 and Klein and Kauahikaua, 1975).

Hydrology

Due to the small population and the poor quality of the water south of the rift zone, there was little interest in the hydrology of Puna prior to geothermal exploration. Since then, several studies have been undertaken but many questions remain. Early descriptions of the hydrology of the area are the main sources of information on the hydrology of the area. Stearns and Macdonald (1946) discuss the occurrence of groundwater and give information on wells and springs prior to 1940. Davis and Yamanaga (1968) summarized current information on the quantity and quality of the water available for water

development. Druecker and Fan (1976) provide the most recent summary of the available hydrology and geochemistry data collected between 1973 and 1975. The Hawaii Department of Water and Land Development (DOWALD, 1970) and U. S. Geological Survey (USGS) reports (Davis and Yamanaga, 1973, Takasaki, 1978, and Groundwater Site Inventory Data File) include information on well locations, water table elevations, quality and temperatures (Table 4 and Figure 5). Drilling logs and pump test data for the Pulama and the Malama-ki wells are summarized in the DOWALD Circulars Numbers 26 and 12 respectively.

The occurrence of groundwater is governed by the geology and the structure of the area (Figure 6). Three types of groundwater are found in Puna: perched, dike confined, and basal waters. Perched water may be locally present on ash beds under the slopes of Kilauea. A pond several meters above sea level in Kapoho Crater may be fed by water perched on poorly permeable tuff (Stearns and Macdonald, 1946). However, perched water bodies tend to be thin and of limited lateral extent, making them unimportant to water development.

Dike confined water is associated with the east rift zone and areas of high local recharge. The low permeability of the dikes cause water to impound to considerable heights above sea level within the rift, while causing depressed water tables downgradient. When dike confinement occurs near sea level and the dikes are parallel to the coast, the rift zone acts as a barrier to the seaward flow of freshwater and the enchroachment of saline waters. In these areas, the freshwater layer does not necessarily continue to the deeper underlying saline water (Stearns and Macdonald, 1946). This anomaly in the normal groundwater conditions may be due to the structure as well as to

Table 4

Well and Shaft Information in the Study Area*

Well No.	Year Drilled	Name	Owner	Lat (W) ' "	Long (N) ' "	Surface Elevation (ft)	Depth (ft)	Use
2487-01 (9-7)	1961	Keauohana	County of Hawaii	19 24 57	154 57 20	751.75	742.47	Domestic
2487-02	1970	Keauohana 2	County of Hawaii	19 24 57	154 57 18	752	803	Domestic
2686-01 (1)	1961	Thermal test well	Hawaii Thermal Power Co.	19 26 34	154 56 46	1009	178	Abandoned
2686-02 (2)	1961	Geothermal test well	Hawaii Thermal Power Co.	19 26 33	154 56 48	1035	556	Abandoned
2783-01 (9-9)	1962	Malama-ki	Hawaii State DOWALD	19 27 28	154 53 01	272.7	319	Unused
2881-01 (A)	1973	Allison	Oneloa Co. Inc.	19 28 19	154 51 10	129	140	Irrigation
2883-01	1975	HGP-A	Kapoho Land and Dev. Co.	12 28 31	154 43 44	600	6450	Geothermal
2982-01 (3)	1961	Geothermal test well	Hawaii Thermal Power Co.	19 29 13	154 52 55	563	690	Abandoned
2986-01 (9-5)	1960	Pahoa	County of Hawaii	19 29 23	154 56 47	704	754	Domestic
2986-02 (9-5B)	1963	Pahoa	County of Hawaii	19 29 24	154 56 47	712	755	Domestic
3080-01 (4)	1961	Geothermal test well	Hawaii Thermal Power Co.	19 30 42	154 50 47	38	46	Abandoned
3080-02 (9)	1965	Kapoho shaft	County of Hawaii	19 30 17	154 50 21	39	46.2	Domestic
3081-01 (9-6)	1960	Airport	Coumty of Hawaii	19 30 25	154 51 59	286.75	337	Domestic
3081-02			Lyman	19 30 39	154 51 19	180	183	Unused
3185-01 (9-11)	1964	Pahoa well 1	Hawn. Parks Inc. Miller-Lieb	19 31 11	154 55 58	402	446	Domestic
3185-02			Hawaiian Shores	19 31 27	154 55 44	380	430	Domestic

*USGS Water Resources Division, Hawaii District Groundwater Site Inventory Data File

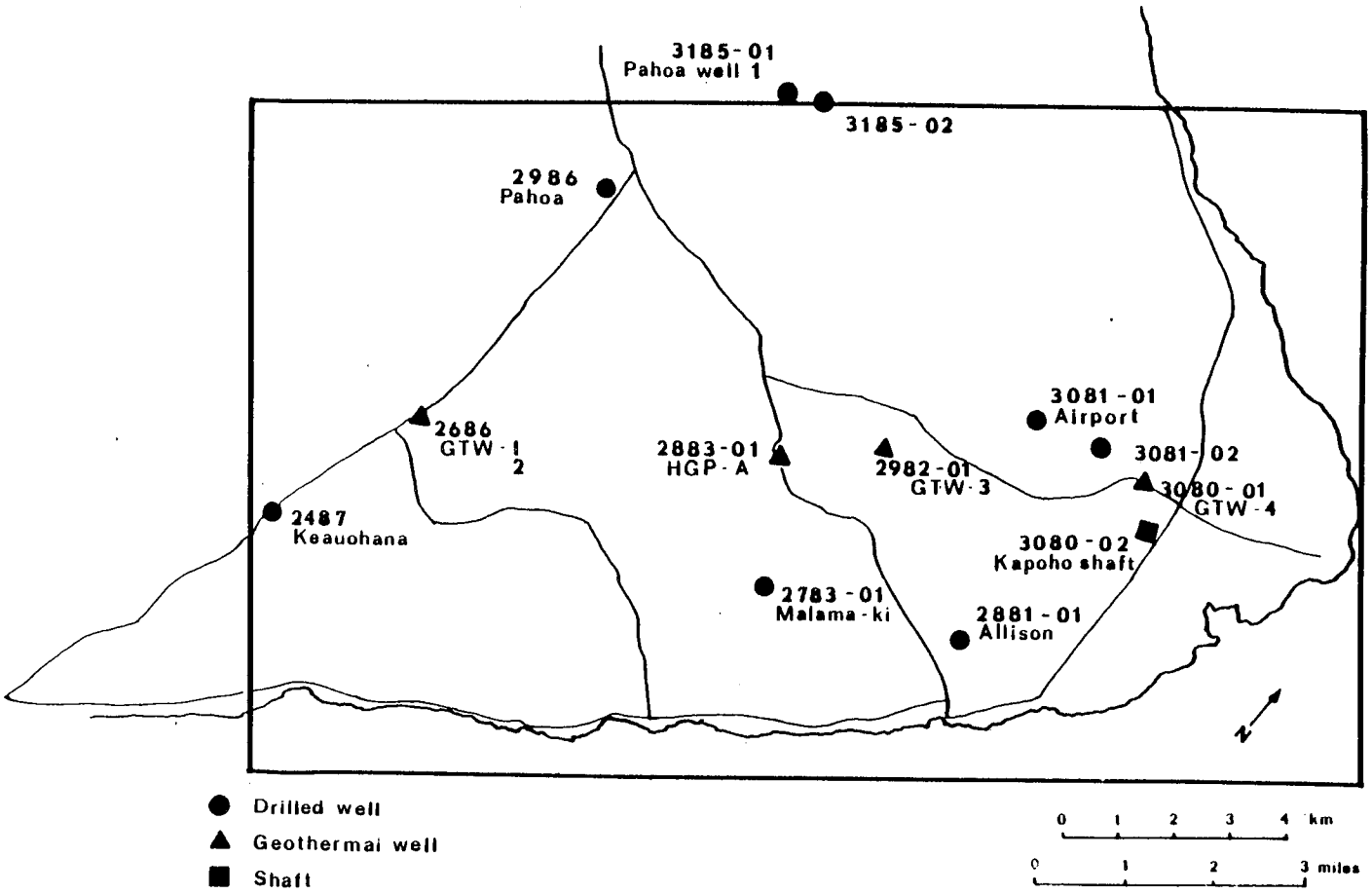

Figure 5. Locations of Wells and Shafts in Puna (DOWALD, 1970)

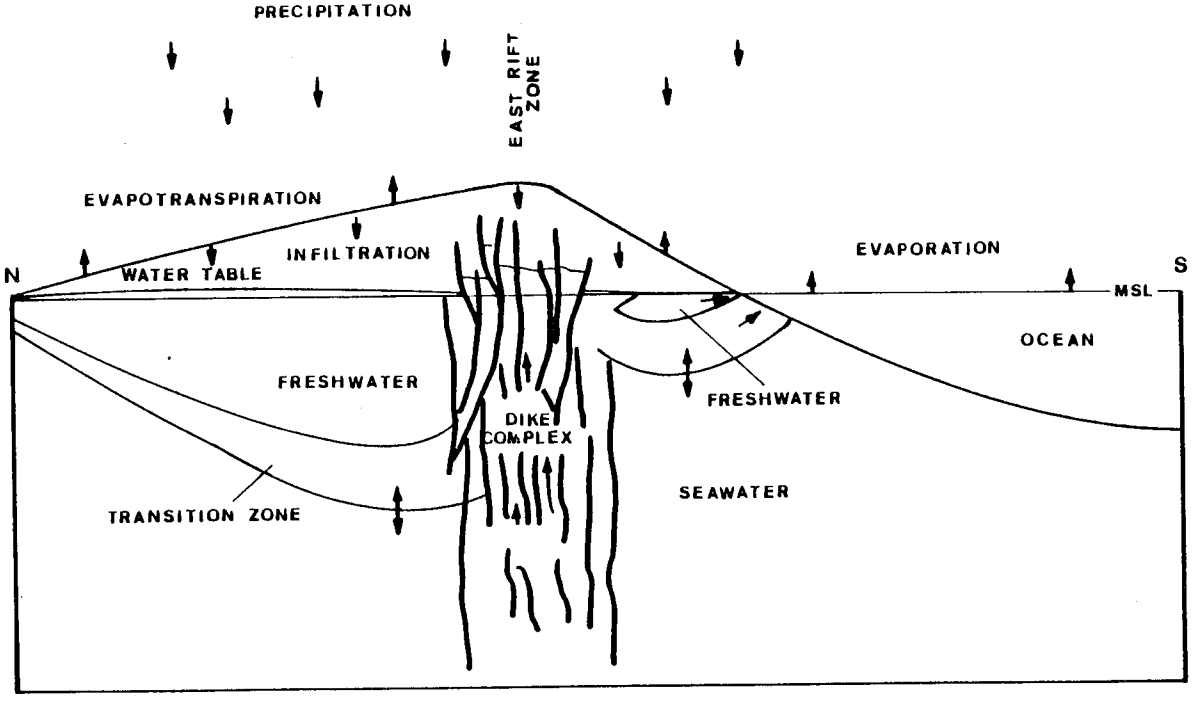

Figure 6. Schematic North-South Cross-Section Through Puna Showing Recharge, Movement, Discharge, Storage, and Subsurface Geology of Groundwater (Druecker and Fan, 1976)

reduction of saltwater density as a result of the higher temperatures to where a basal freshwater lens can no longer be supported (Furumoto et al., 1977).

Basal water lies under all of Puna in the form of a Ghyben-Herzberg lens, with the exception of the rift zone where water is impounded to great heights. North of the rift basal water has normal temperature and low salinity, while south of the rift the water is abnormally warm and saline.

HGP-A was drilled in the east rift zone to a depth of 1966 m. The well was cased to a depth of about 692 m, below which a slotted liner was used to allow the inflow of fluids. Unfortunately the height of the head is unknown, so the extent of impoundment cannot be determined. The HGP-A well water is fresher than the surrounding wells and its chemical composition varies very little with depth (Kroopnick et al., 1978). Although small zones of high permeability exist, the major production zone is between 1387 to 1905 m (Yuen et al., 1978).

The hydraulic gradient and the permeability govern the seaward flow of the fresh basal water. Figure 7 shows the water table elevations. Along the northeastern coast of Puna hydraulic gradients range between 0.38 and 0.76 meters per kilometer (2-4 ft/mi), with groundwater elevations of 3.66 to 5.49 meters (12-18 ft) above sea level 8.05 to 9.66 kilometers (5-6 mi) inland. Along the southeastern coast gradients range between 0.19 and 0.38 meters per kilometer (1-2 ft/mi), with basal water elevations of 0.91 to 1.22 meters (3-4 ft) 2.41 kilometers (1.5 mi) inland. The major reason for the difference in the gradients is the barrier effect of the east rift zone (Druecker and Fan, 1976).

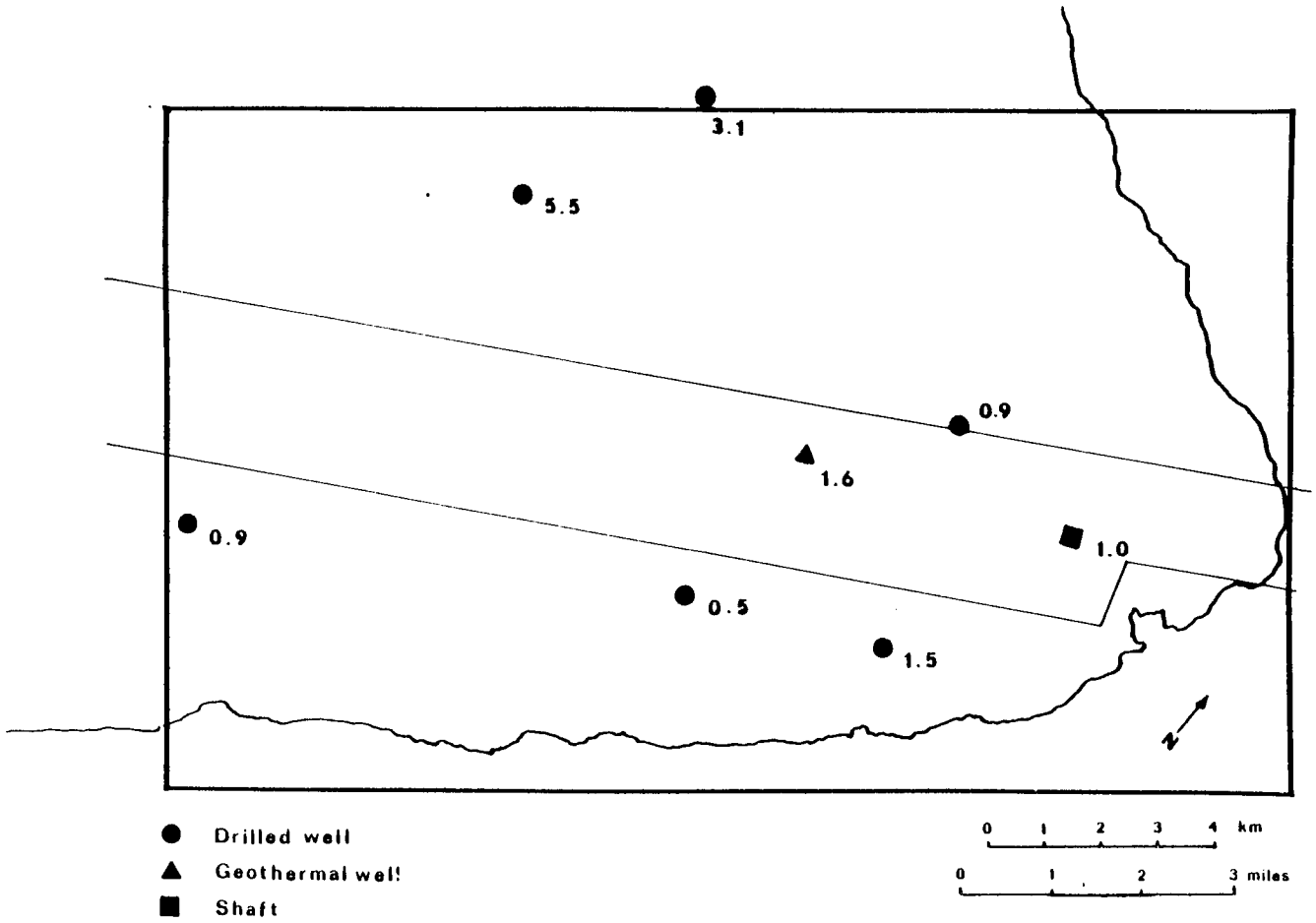

Figure 7. Average Heads in Meters Above Sea Level
(See Appendix A)

Water moves through the permeable basalts via four major types of conduits: joints, interflow layers, aa clinker layers and lava tubes. A large range of permeabilities exist in Puna. The permeability near the surface is very high, averaging 4000 to 5000 darcies (3.9×10^{-5} - 4.9×10^{-5} cm^2) (Druecker and Fan, 1976). The permeability decreases with depth depending on joints and fractures. Below 1830 meters, the pillow basalts have permeabilities on the order of a few millidarcies (9.9×10^{-12} cm^2) (Yuen et al., 1978).

Average transmissivities on the order of 10^5 millidarcy-ft (2.5×10^{-3} m^2/d) are estimated for the shallow Puna wells (Kroopnick et al., 1978). However, the transmissivity of the rift zone is significantly lower, the formation transmissivity found in HGP-A was found to be between 1000 and 1500 millidarcy-ft (2.5×10^{-1} - 3.8×10^{-1} m^2/d) (Yuen et al., 1978).

The relatively thin soil layer, minimal interlayered ash, and high hydraulic conductivities allow most of the rainfall to percolate rapidly downward resulting in the absence of any surface waters. Assuming that little surface runoff occurs, the amount of recharge can be directly related to rainfall, and water available for recharge can be calculated from data gathered from rainfall stations (Figure 8). Davis and Yamanaga (1968) estimated the rate of recharge from precipitation in Puna to average 1.2×10^7 m^3/day (3,140 MGD). Of this, approximately 1.1×10^7 m^3/day (2,830 MGD) of rainfall infiltrates into the basal lens. The remaining 1.2×10^6 m^3/day (310 MGD) is evapotranspirated.

The basal groundwater is discharged along the coasts in the form of diffuse flows and a few large basal springs. Along the northeastern coast, the

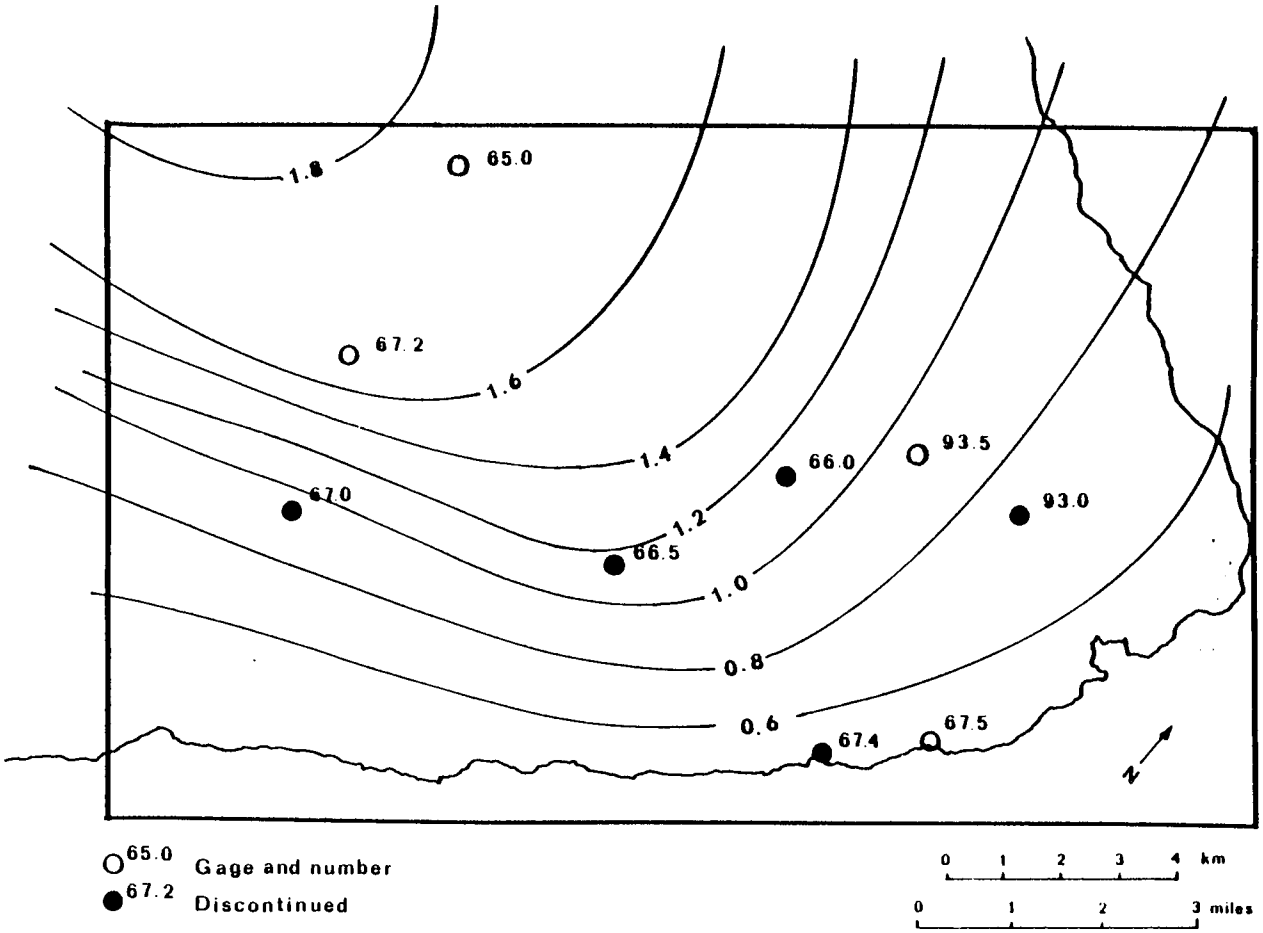

Figure 8. Annual Recharge from Precipitation in Meters (Imada, 1982)

daily groundwater discharge is estimated to be on the order of several million gallons (Davis and Yamanaga, 1968). The discharge along the southeastern coast, however, is much lower. Sparse thermal anomalies along this shore suggest that the discharging groundwater is warmer than the surrounding seawater (Fischer et al., 1964).

The basal lens yields water easily to wells. Well yields of more than 1.1 m^3/min (300 gpm) per foot of drawdown are common and some yield 1.9 to 3.8 m^3/min (500-1000 gpm) (Davis and Yamanaga, 1968). Nonetheless, discharge of groundwater through wells is relatively low because only four wells tap the basal groundwater in the area: well no. 9.5a pumps 7.2 x 10^7 m^3 annually (18.9 MG), well no. 9.5b pumps 1.8 x 10^5 m^3 annually (48.3 MG), well 9.6 pumps 2.2 x 10^4 m^3 annually (5.7 MG), and well 9-7 pumps 4.1 x 10^4 m^3 (10.9 MG) annually (Dept of Water Supply, 1971-1981).

Temperature and Chemistry

The distribution of water temperatures for the wells in Puna are shown in Figure 9. As expected, the groundwater temperatures are significantly affected by the east rift zone. Well water temperatures north of the rift are normal, ranging from 18 - 23°C, but south of the rift, temperatures greater than 26 °C are common. This suggests that warm water is escaping from the dike complex into the basal groundwater to the southeast.

Vertical water temperature profiles in shallow wells were measured by Epp and Halunen (1979). The groundwater temperatures varied very little with depth for most of the shallow wells. However, GTW-3 (2982-01) and to a lesser extent Malama-ki (2783-01) showed a decrease in temperature near the bottom of

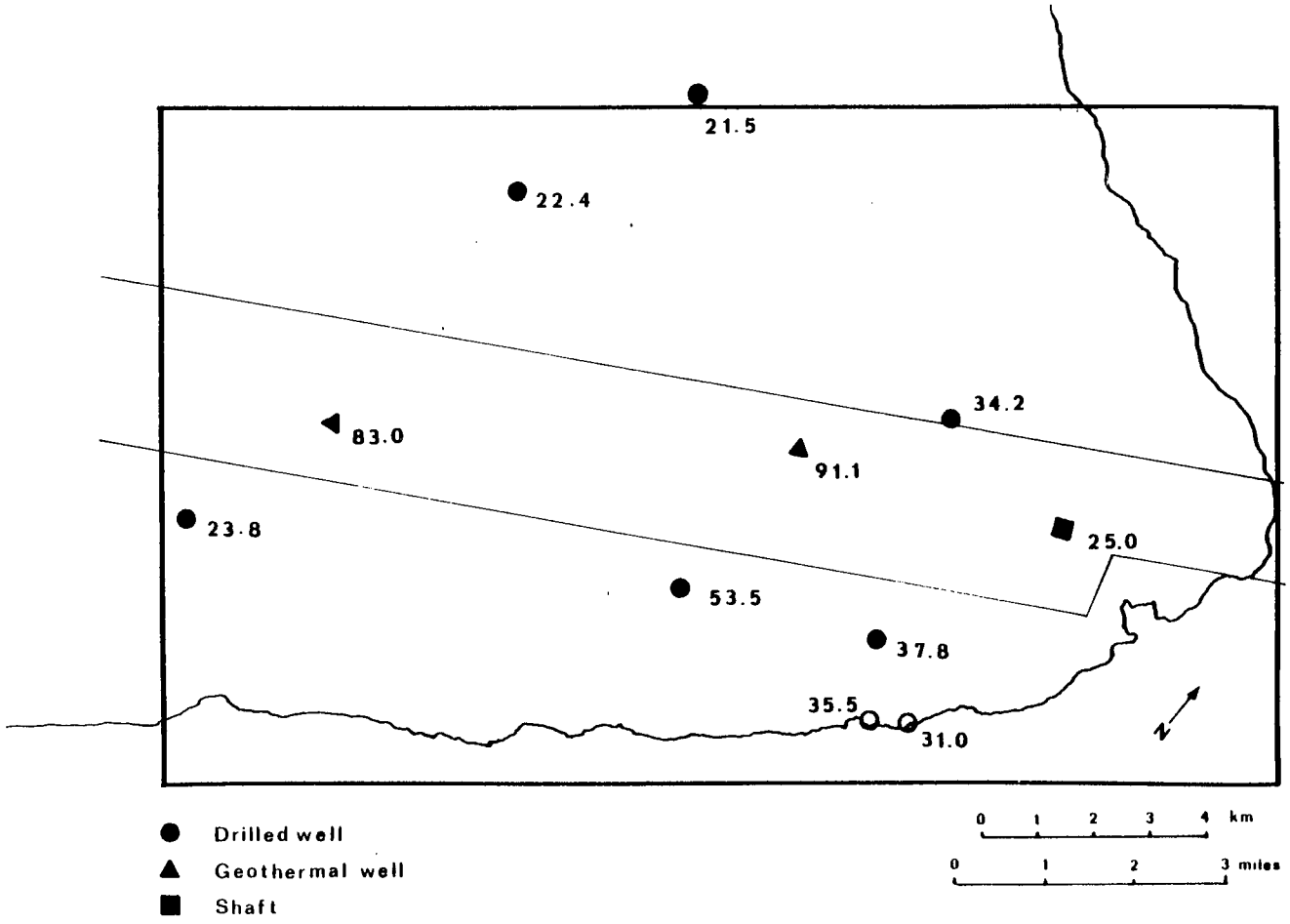

Figure 9. Average Temperatures in °C
(See Appendix B)

the well suggesting that a thermal region exists upgradient. They concluded that residual heat exists within the upper few hundred meters and varies along the rift. In GTW-3 (2982-01), the surface waters are not only hotter but more saline than the underlying waters (Buddemier et al., 1976). This may be a result of thermal density inversions where the warmer saline water floats above the colder meteoric water and may account for the high salinities of the warm water wells (Thomas et al., 1979).

The chemistry of Hawaiian groundwater is highly localized. The main controls on the chemistry are the aquifer type, soil cover, surface land usage and recharge-discharge rates. On the younger islands like Hawaii, the high recharge and basal discharge allow only minimal rock water interactions. Therefore, under normal conditions the silica concentrations should be relatively low. Since seawater enchroachment is the major source of salts, the concentrations of salts inland should also be low (Thomas et al., 1979).

However, the mechanisms controlling the geochemistry of the water in Puna are slightly more complex. As shown in Figure 10, the samples of groundwater collected here are predominantly of the sodium chloride type, where sodium and chloride comprise the majority of the ions in milliequivents. However, there are two exceptions. The water from the Kapoho Shaft (3080-01) is considered to be calcium magnesium sodium bicarbonate type since all of the ions are found in nearly equal proportions. The high bicarbonate concentrations are thought to be an indication of volcanic gases at this location. The water of the Pahoa well (2986-01) is designated as the sodium bicarbonate type which shows the small influence of seawater at this distance inland (Swain, 1973).

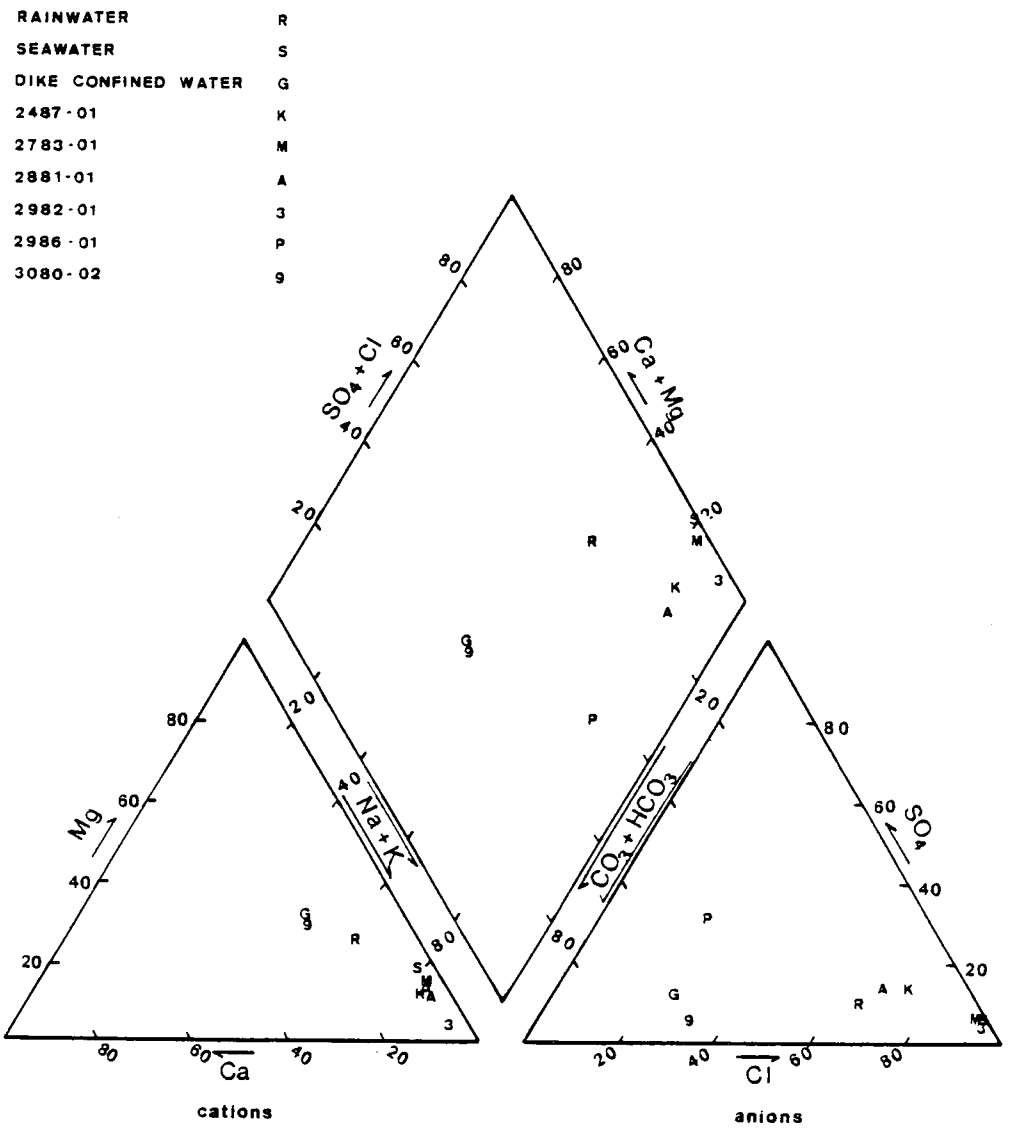

Figure 10. Chemistry of Groundwater from Puna Wells (Kroopnick et al., 1978)

The east rift zone acts as a divide for salinity (Figure 11). North of the rift zone chloride concentrations are relatively low, while south of the rift zone chloride concentrations greater than 1000 milligrams per liter (mg/l) are common (Davis and Yamanaga, 1968). The higher salinities may be due to several factors including the heat induced mixing of the seawater and the basal lens, the barrier affects of the rift zone reducing the amount of freshwater through the area, and the low amounts of recharge along the southeastern coast.

The major ions in the water chemistry are dependent upon the water temperature. Silica content, normally 30 mg/l for Hawaiian waters, increases with higher temperatures to concentrations up to 100 mg/l (Figure 12). In general, as temperatures increase, the sodium and potassium concentrations increase while calcium and magnesium concentrations decrease. This is thought to be due to the high temperature water-mineral reactions occurring in the aquifer (Kroopnick et al., 1978). The magnesium and calcium are removed from seawater to form chlorite and anhydrite respectively, as suggested by the rock cores from HGP-A (Thomas and Sakai, 1983)

Concentrations of tridium and $\delta^{18}O$ indicate that the mean residence time of shallow groundwaters does not exceed a few tens of years (Kroopnick et al., 1978). This rapid turnover confirms that the hydraulic conductivities of the shallow aquifer must be relatively high to sustain the necessary flow.

The reservoir tapped by HGP-A is separted from the shallow groundwater by an impermeable layer and, consequentially, is considered to be different from the groundwater. The reservoir fluid is much fresher than would be predicted by the Ghyben-Herzberg relationship. The barrier affect of the dike system

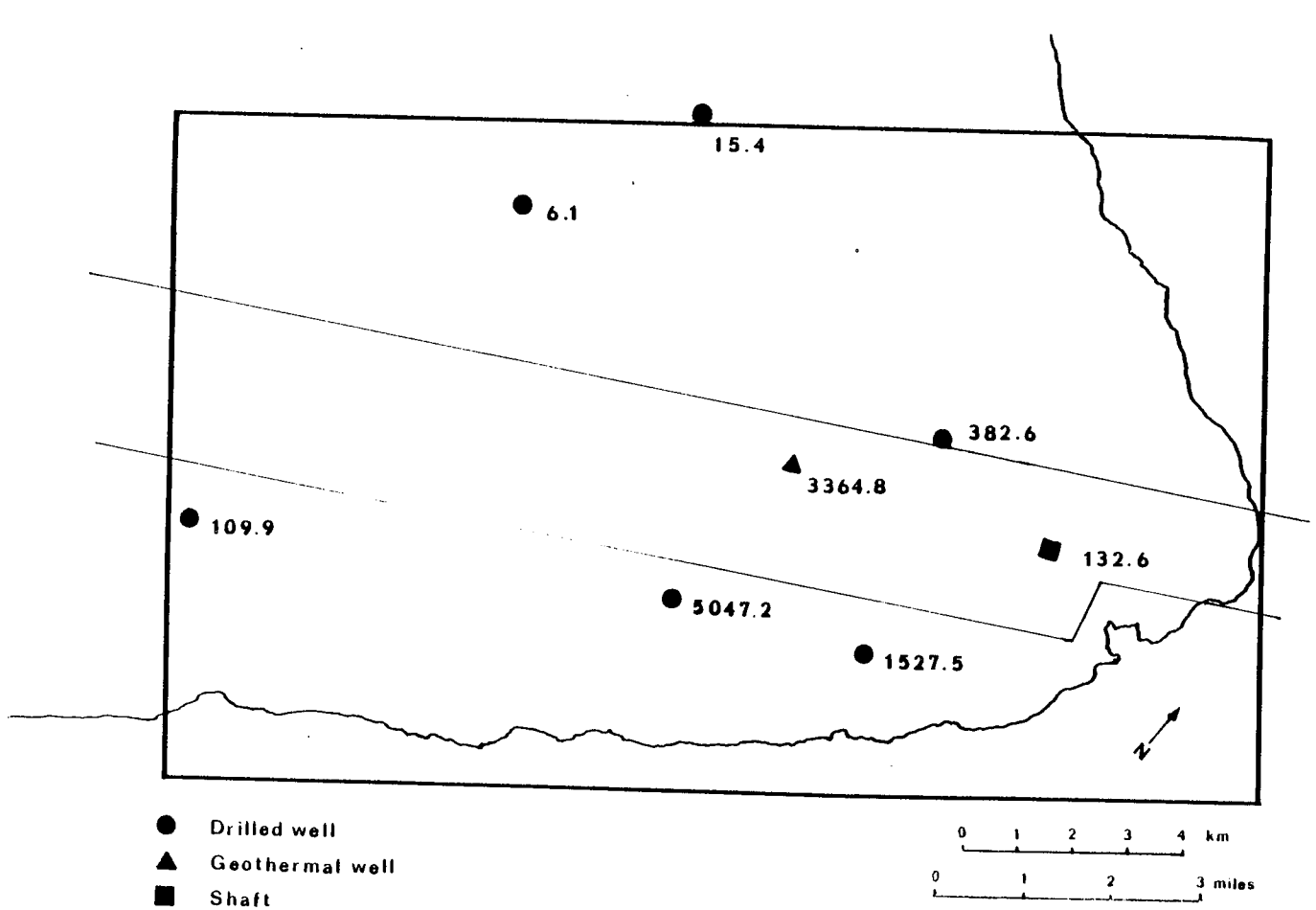

Figure 11. Average Chloride Concentrations in ppm
(See Appendix C)

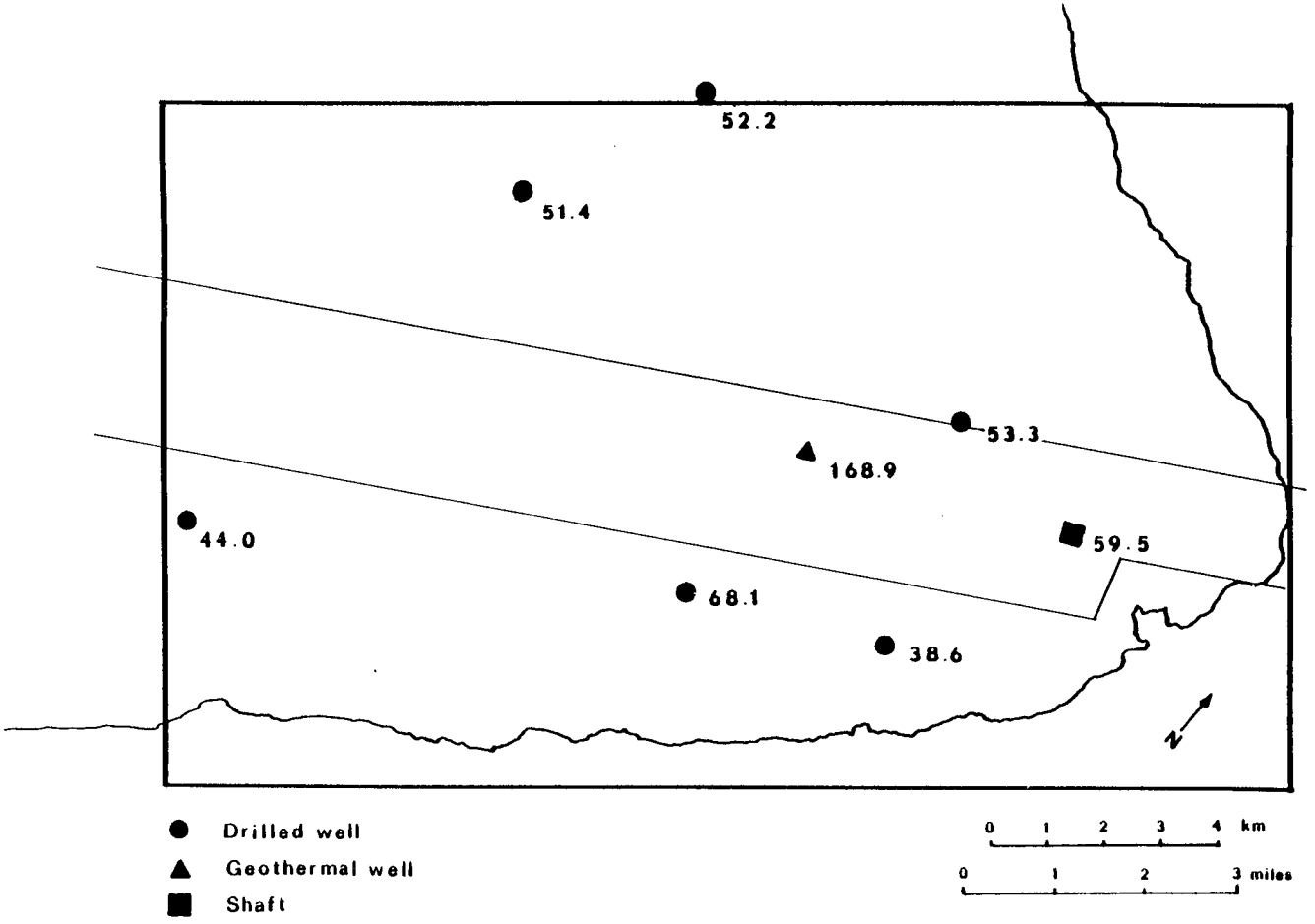

Figure 12. Average Silica Concentrations in ppm
(See Appendix D)

constrains the encroachment of seawater into the rift zone. The precipitation of anhydrite and other secondary minerals from the infiltrating seawater causes the reservoir to be self-sealing and further restricts the flow across the rift (Thomas and Sakai, 1983). The fluid in the reservoir contains about 10% seawater, 66% groundwater, and 24% hydrothermally altered fluids with a deep-seated or magmatic source (Kroopnick et al., 1980). The fluids have an estimated maximum age of 12,000 years (Thomas and Sakai, 1983). Table 5 shows the chemistry of the fluids of the geothermal reservoir fluids over time. The increases in chloride, sodium, and potassium seem to suggest that the seawater influx into the reservior has increased (Thomas and Sakai, 1983).

Table 5

Chemical Composition of the HGP-A Reservoir Fluids*

Date	Cl	Na	K	Mg	Ca	SiO_2	CO_2	H_2S
1- 8-76	876	480	84.8	0.2	32.8	-	-	-
4-11-77	1220	584	106.4	0.1	30.9	404	-	-
6-12-81	637	322	61.6	0.021	7.4	408	600	450
9- 4-81	2109	1248	143	0.06	41.0	456	538	409
4-19-82	3017	1591	269	0.076	70.1	455	559	387
7-12-82	3445	1881	306	0.041	89.5	466	540	389
2-15-83	4260	2883	373	0.087	142.5	-	-	-
4-18-83	4392	2883	366	0.096	156.	467	538	412.8

* From Thomas and Sakai, 1983

CHAPTER III

NUMERICAL MODELING

Related Studies

Modeling in General. The use of numerical modeling has become especially significant in groundwater resource management. The methods used add significant insight to the development and the protection of the water resources available.

The numerical modeling of groundwater flow and solute transport involves solving a set of partial differential equations that describe the system. Faust and Mercer (1980) give a good general overview of the various methods commonly used in groundwater studies. Slightly more mathematical presentations of different numerical schemes are given in Freeze and Cherry (1979) and by Bear (1979). Specialized sources include Remson et al. (1971), who concentrate on finite difference methods in model solution, Pinder and Gray (1977) who deal mainly with the finite element method and Wang and Anderson (1982) who describe both methods for use in hydrology. Breddia (1978) and Carnahan et al. (1969) are good references for the numerical solutions of partial differential equations. Detailed descriptions of available models for groundwater management are given by Bachmat et al. (1980).

Solution to the Flow Equation. A major concern in water resource management is the quantity of water available. To study this, numerical methods to solve the flow equation for different boundary and initial conditions have been developed. Derivation of the flow equations are given in Bear (1979) and Freeze and Cherry (1979).

The numerical models developed are capable of predicting the aquifer response to various stresses due to different patterns of recharge and withdrawal. Many of the two-dimensional models such as those constructed by Pinder and Bredehoeft (1968) or Trescott et al. (1976) can accomodate various aquifer types, inhomogeneities, anisotropy, leakage and well discharge. The parameters are usually averaged in the vertical direction however. Bredehoeft and Pinder (1970) developed a quasi-three-dimensional model to simulate flow through the confining layers of multiple aquifer systems.

Solution to the Mass Transport Equation. Quality of available water resources is also of concern. Stresses on the aquifer due to waste injection, agricultural pollution, and salt water intrusion have been analyzed using the mass transport equation (Fried, 1975). To incorporate quantity as well as quality of groundwater, the flow equation is coupled to the mass transport equation. Such water quality models contain a flow submodel which computes the velocities in the system. The velocities are then used in a mass transport submodel which moves the contaminants in the flow field, allowing for dispersion and transformation by reactions.

Many of the earlier developments in water quality modeling dealt basically with the problem of saltwater intrusion or the location of the saltwater interface. Several modeling schemes exist to study these problems. Dagan and Bear (1968) used the method of small perturbations to approximate the local upconing of the freshwater-saltwater interface due to pumping from a coastal aquifer. The method of characteristics was used by Pinder and Cooper (1970) to simulate the transient saltwater interface considering the effects of dispersion. Shamir and Dagan (1971) and Mercer et al. (1980) both modeled

the interface location by vertical integration. Models to examine these problems are still being modified or developed as seen;in recent articles by Kembloski (1983), Das Gupta and Yapa (1982), and Polo and Ramis (1983).

The problem of waste disposal has also initiated several modeling studies. Redell and Sunada (1970) developed a two-dimensional model to simulate the dispersion of a conservative contaminant in an isotropic medium. This study also considered the tensorial nature of the dispersion coefficient. Modeling of waste injection into a Ghyben-Herzberg system was undertaken by Wheatcraft and Peterson (1979). Other quality problems were studied by Bredehoeft and Pinder (1973) and Konikow and Bredehoeft (1974) who analyzed the salinity increases in an aquifer due to irrigation practices.

Many water quality models exist as described by Bachmat et al. (1980). One of the most useful, a two-dimensional model presented in very general and flexible terms such that it can be applied to many different problems, has been developed by Konikow and Bredehoeft (1978).

Groundwater Modeling in Hawaii. Water budget models, flow models, mass transport models, and thermal models have been used in studies of Hawaiian groundwater. The water budget approach balances the total input, output, and changes in storage in an aquifer to estimate the freshwater flux through the system. Kanehiro and Peterson (1977) developed a water budget model to calculate the average annual recharge and freshwater discharge along the northwestern coast of the Island of Hawaii. As a result, daily flux of 15,006 cubic meters per kilometer (6.38 million gallons/mile) of coastline was estimated. Hydraulic conductivities of 2,771 m/day (9,092 ft/day) were

calculated compared with 1,027 m/day (3,369 ft/day) determined by a tidal analysis method.

Eyre (1977) used the water budget approach to calculate the amount of recharge from precipitation over a 2.6 km^2 area (one mi^2) centered around the HGP-A well (Puna, Hawaii). He modeled found that the amount of recharge available would be about one order of magnitude greater than the anticipated flow-rate of the HGP-A well.

Water budget models are most useful only if an estimation of groundwater flux is needed. They do not take into account the detailed hydrogeology of the system. Since the model is simply a budgeting of inputs and outputs, it cannot consider the local variability of the hydrology or the well discharges. Therefore, other techniques must be utilized to get a more reasonable picture of the aquifer system.

Groundwater flow models attempt to simulate the regional flow of the aquifer system. Liu et al. (1983) used the two-dimensional model developed by Trescott et al. (1976) to study the Pearl Harbor aquifer on Oahu, Hawaii. The model simulated the evolution of the freshwater lens and the effects of long term pumping on freshwater storage. The hydraulic conductivities used in this study ranged between 305-610 m/day (1000-2000 ft/day).

Imada (1982) used a similar model to describe the groundwater flow in Puna on the Island of Hawaii. The model tried to reproduce the effects of Kilauea's east rift zone on groundwater flow. Hydraulic conductivities in this study were estimated to be 4000 m/day in the non-rift areas and 10 m/day for the rift areas.

These flow models answer many questions about the quantity and regional flow of groundwater under different hydrologic conditions. However, due to the problem of seawater intrusion and upconing of the seawater interface in coastal aquifers, water quality is also a significant consideration in resource management. Effects of density changes due to salinity and heat on groundwater flow should be analyzed in the modeling of Hawaiian aquifer systems.

To study the effects of pumping on the transition zone a mass transport model was used by Liu et al. (1984). The model by Konikow and Bredehoeft (1978) was adopted in their study to simulate the response of the Beretania basal-water body in southern Oahu, Hawaii. The periods of interest include the predevelopment years (before 1890) and from 1930 to 1960 when the aquifer was considered to be at steady state. A dispersion coefficient of 0.21 m^2/d (0.7 ft^2/day, dispersivity of 0.76 m or 2.5 ft) was estimated by comparing the observed salinity profile with the model results. The relationship between outflow and the head behind the caprock was also established.

Cheng and Lau (1978) conducted a study to investigate heat transfer and fluid flow characteristics of the geothermal reservoir in Puna. They constructed a numerical model simulating convection in a multi-layered geothermal reservoir, with recharge and discharge through an upper permeable boundary. The model gave temperature profiles strongly resembling the profiles observed in HGP-A. Only the effect of heat on the water in the geothermal reservoir was considered and the effect of the temperature on the upper groundwater system or effects of density changes due to chemistry were not examined.

Mathematical Formulation

This study is a first attempt to incorporate the effects of groundwater flow, temperature and chemistry in a numerical model of Puna. The model will be divided into two submodels. The first, the flow submodel, will use values for recharge, intrinsic permeability, temperature, well discharge, and thickness to calculate the head distribution (see Figure 13a). The transport submodel will be used to calculate the distribution of a specified chemical species at a particular time (see Figure 13b). The results of the model will be calibrated using observed well data. Once the model has been calibrated, the affects of geothermal activity on the groundwater will be examined.

The accuracy of the results of this model will depend on the initial assumptions and simplifications made in the development of this numerical study. Although the derivation of the flow and transport equations can be found in Bear (1972 and 1979) or Freeze and Cherry (1979) as well as many other sources, the formulation of the equations are presented here to delineate the important assumptions made.

Flow Equation. The flow of water in an aquifer can be expressed by a partial differential equation based on the laws of mass conservation. Following the derivation of the flow equation by Bear (1972), the three-dimensional flow of water in an aquifer may be written in vector notation as

$$\nabla \cdot (\rho q) = \frac{\partial}{\partial t} (\alpha \rho) \qquad [1]$$

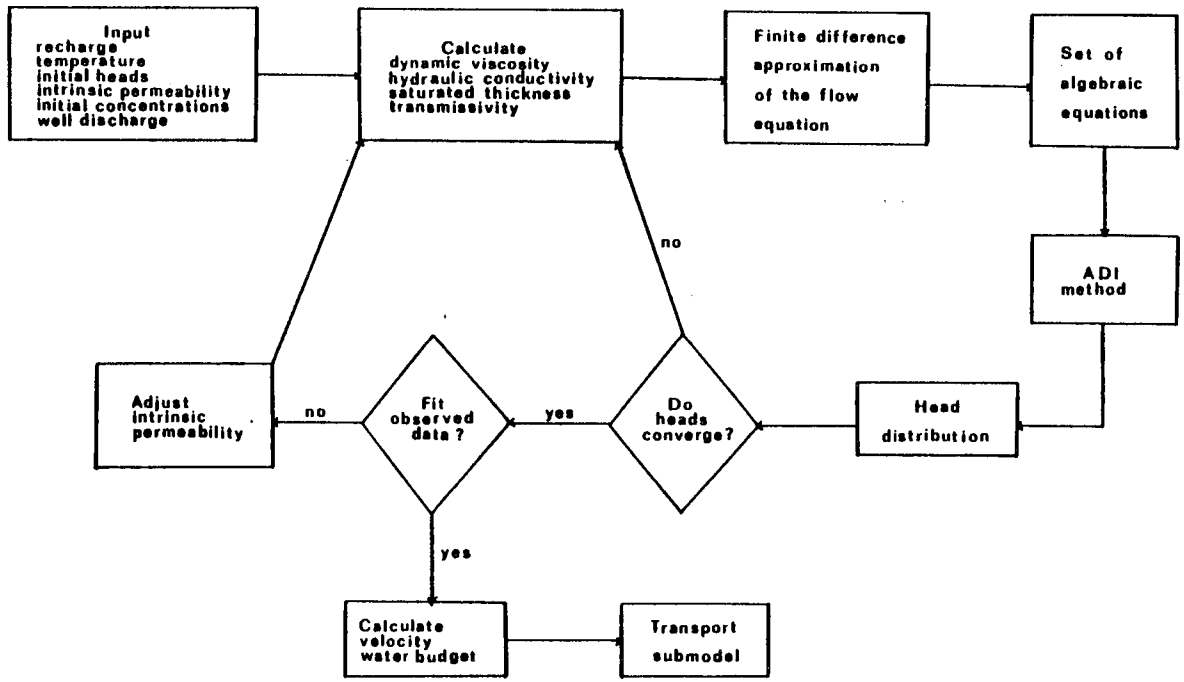

Figure 13a. Simplified Flow Diagram of the Flow Submodel

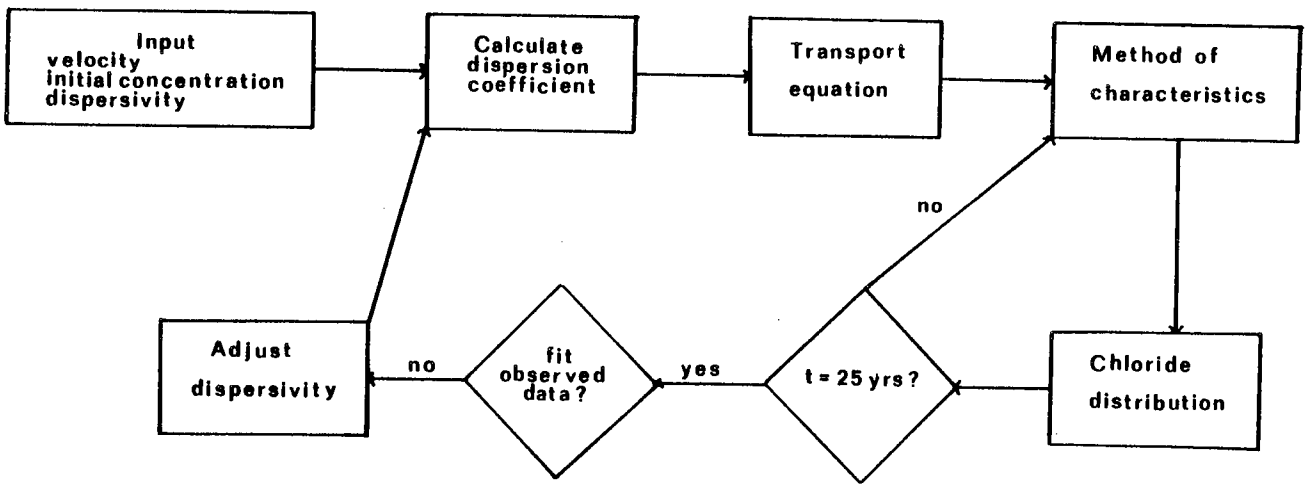

Figure 13b. Simplified Flow Diagram of the Transport Submodel

where

ρ is the density of water (M/L^3);

q is the specific discharge (L/t);

α is the porosity (dimensionless);

t is the time dimension (t); and

∇ is the vector operator.

If the fluid and the aquifer are considered to be compressible, the right-side of the equation can be expressed as a function of the specific yield of the aquifer, Sy (dimensionless), and the hydraulic head, h (L).

Equation 1 becomes

$$\nabla \cdot (\rho q) = - \rho Sy \frac{\partial h}{\partial t} \qquad [2]$$

Groundwater flow is a three-dimensional, transient problem. However, due to the complexity and the cost of computer simulations, this study is confined to analyzing steady state flow in a horizontal plane of thickness, b (L). The parameters are averaged in the vertical direction.

The specific discharge can be expanded using Darcy's law.

$$q_i = (-Kb)_{ij} \frac{\partial h}{\partial x_j} \qquad [3]$$

in which

K_{ij} is the hydraulic conductivity tensor (L/t);

b is the saturated thickness (L); and

x is the Cartesian coordinate (L).

The flow equation can be written as

$$\nabla \cdot \left[(\rho Kb)_{ij} \frac{\partial h}{\partial x_j} \right] = \rho Sy \frac{\partial h}{\partial t} \qquad [4a]$$

or in Cartesian tensor notation as

$$\frac{\partial}{\partial x_i} \left[(\rho Kb)_{ij} \frac{\partial h}{\partial x_j} \right] = \rho Sy \frac{\partial h}{\partial t} \qquad [4b]$$

The hydraulic conductivity reflects the ease with which water can move through a porous media. Hence, the hydraulic conductivity depends on both the properties of the fluid as well as those of the media. The fluid properties considered are the density and vicosity of the fluid, while the pore size distibution, porosity and tortuosity are the properties of the media. Expanding the hydraulic conductivity into its components gives

$$K_{ij} = k_{ij} \frac{\rho g}{\mu} \qquad [5]$$

where

k_{ij} is the intrinsic permeability tensor (L^2);

μ is the dynamic viscosity (M/Lt); and

g is the acceleration due to gravity (L/t^2).

Since the dynamic viscosity is related to the fluid termperature in degrees Celsius, T, by (Handbook of Chemistry and Physics, 1972)

$$\log \frac{\mu_T}{1.002} = \frac{1.3272(20-T) - (0.001053(T-20)}{T + 105} \qquad [6]$$

This allows some of the temperature effects on groundwater flow to be incorporated into the model.

The intrinsic permeablity, k_{ij}, is a second rank tensor, which varies as a function of direction. In this study, it is assumed that the principal directions of the intrinsic permeability tensor are aligned with the coordinate axis or

$$k_{ij} = \begin{bmatrix} k_{11} & 0 \\ 0 & k_{22} \end{bmatrix} \qquad [7a]$$

This implies that all flow will be along a principal direction. However, the media will be considered to be isotropic with respect to intrinsic permeability or

$$k_{ij} = k \begin{bmatrix} 1 & 0 \\ 0 & 1 \end{bmatrix} \qquad [7b]$$

The flow has been considered to be density dependent. In a horizontal model, the local and temporal changes in density are much larger than the regional variations. The flow equation in the form of Equation 4b will be used to demonstrate this. Recall that

$$\frac{\partial}{\partial x_i} \left[(\rho Kb)_{ij} \frac{\partial h}{\partial x_j} \right] = \rho Sy \frac{\partial h}{\partial t} \qquad [4b]$$

The equation for the hydraulic head for a compressible fluid is

$$h = \int_{P_o}^{P} \frac{dP}{\gamma} + z \qquad [8a]$$

or

$$h = \frac{\nabla P}{\rho g} + z \qquad [8b]$$

where

P is the pressure (F/L^2);

z is the elevation above some datum (L); and

γ is the specific weight of water (F/L^3).

Substituting for the heads and expanding the hydraulic conductivities gives

$$\frac{\partial}{\partial x}\left[\frac{\rho}{\mu} k_{11}\, b \frac{\partial P}{\partial x}\right] + \frac{\partial}{\partial y}\left[\frac{\rho}{\mu} k_{22}\, b \frac{\partial P}{\partial y}\right] + \frac{\partial}{\partial z}\left[\frac{\rho}{\mu} k_{33}\, b \frac{\partial P}{\partial z}\right]$$

$$+ \frac{\partial}{\partial z} \frac{\rho^2 g}{\mu} k_{33}\, b = -\rho Sy \frac{\partial h}{\partial t} \qquad [9a]$$

However, in this study, everything is assumed to be constant in the vertical direction thus

$$\frac{\partial P}{\partial z} = 0 \quad \text{and} \quad \frac{\partial}{\partial z} \frac{\rho^2 g}{\mu} k_{33} = 0 \qquad [9b]$$

and therefore

$$\frac{\partial}{\partial x} \frac{\rho}{\mu} k_{11}\, b \frac{\partial P}{\partial x} + \frac{\partial}{\partial y} \frac{\rho}{\mu} k_{22}\, b \frac{\partial P}{\partial y} = -\rho Sy \frac{\partial h}{\partial t} \qquad [9c]$$

This is essentially equivalent to the flow equation in terms of head (Equation 4b). Hence, in the plan-view model the dependence of density need not be considered. Equation 4b can be simplified to

$$\frac{\partial}{\partial x_i} [(Kb)_{ij} \frac{\partial h}{\partial x_j}] = Sy \frac{\partial h}{\partial t} \qquad [10]$$

To solve the flow equation some estimate of the saturated thickness must be made. Assuming the existence of the Ghyben-Herzberg lens, the

fresh-saltwater interface can be determined as a function of the hydraulic heads (Hubbert, 1940).

$$z = \frac{\rho}{\rho_s - \rho_f} h_s - \frac{\rho}{\rho_s - \rho_f} h_f \qquad [11a]$$

where

z is the interface location below sea level (L);

h_s is hydraulic head in the saltwater measured below sea level (L);

h_f is the hydraulic head in the freshwater measured above sea level (L);

ρ_s is the density of saltwater (M/L^3); and

ρ_f is the density of freshwater (M/L^3).

Since the saltwater movement is small in comparison with the freshwater, the saltwater head term can be ignored (Liu et al., 1983). The equation becomes

$$z = \frac{\rho}{\rho_s - \rho_f} h_f \qquad [11b]$$

and the saturated thickness can then be calculated by

$$b = z + h \qquad [11c]$$

The flow equation as written in Equation 10 does not account for input or discharge from the aquifer. Therefore, another term, $W(x,y,t)$ which represents the volumetric flux of recharge or removal per unit surface area of the aquifer (L/t) is necessary. The flow equation then becomes

$$\frac{\partial}{\partial x_i}\left[(Kb)_{ij}\frac{\partial h}{\partial x_j}\right] = Sy\frac{\partial h}{\partial t} + W(x,y,t) \qquad [12]$$

The term W(x,y,t) can be expanded

$$W(x,y,t) = \frac{Q_w}{\partial x \, \partial y} - q_{re} \qquad [13]$$

in which

Q_w is the well discharges (L^3/t);

q_{re} is the diffuse recharge per unit area (L/t); and

∂x, ∂y is the space increment (L).

Equation 12 constitutes the fundamental equation for the formulation of the flow portion of this model. Before solving any of these equations, proper boundary and initial conditions must be defined.

Transport Equation. The two-dimensional transport and dispersion of a nonreactive solute in a porous media is governed by the conservation of mass and Fick's law. The derivation of the transport equation can be found in Bear (1972), Fried (1975), and Fischer et al. (1979). The conservation of mass equation can be written as

$$\frac{\partial bC}{\partial t} = \frac{\partial bF}{\partial x_i} + \frac{C'W}{\varepsilon} \qquad [14]$$

where

C is the concentration of the dissolved chemical species in the aquifer (M/L^3);

F is the flux of the fluid movement (M/tL^2); and

C' is the concentration of the dissolved chemical in a source or sink fluid (M/L^3)

ε is the effective porosity

h, t, W are as previously defined

The rate of mass transport, F, can be attributed to two mechanisms. The first, advection, is dependent on the velocity of the fluid.

$$\text{Transport by advection} = V_i \times C \qquad [15a]$$

in which

V_i is the average fluid velocity where

$$V_i = \frac{K_{ij}}{\varepsilon} \frac{\partial h}{\partial x_j} \qquad [15b]$$

The second transport mechanism is the hydrodynamic dispersion. Fick's law states that the solute flux by dispersion is proportional to the gradient of the solute concentration or

$$\text{Transport by dispersion} = - D_{ij} \frac{\partial C}{\partial x_j} \qquad [16]$$

where

D_{ij} is the dispersion coefficient (L^2/t)

Therefore, the total solute mass flux is

$$F = V_i C + \left(- D_{ij} \frac{\partial C}{\partial x_j} \right) \qquad [17]$$

Substituting for F in the mass conservation equation gives the diffusion equation

$$\frac{\partial Cb}{\partial t} = \frac{\partial}{\partial x_i} \left(bD_{ij} \frac{\partial C}{\partial x_j} \right) - \frac{\partial}{\partial x_i} (bCV_i) - \frac{C'W}{\varepsilon} \qquad [18]$$

The hydrodynamic dispersion coefficient is a second-order tensor which may be related to the velocity and the character of the aquifer by (Scheidegger, 1961)

$$D_{ij} = \alpha_{ijmn} \frac{V_m V_n}{|V|} \qquad [19]$$

where

α_{ijmn} is the dispersivity of the aquifer (L);

V_m and V_n are the components of velocity in the m and n directions (L/t); and

$|V|$ is the magnitude of the velocity (L/t)

In porous media, the dispersion occurs parallel as well as transverse to the mean direction of flow. If the aquifer is considered isotropic, the longitudinal and the transverse dispersivities can be assumed constant. The longitudinal and transverse dispersion coefficients may be expressed as (Scheidegger, 1961)

$$D_L = \alpha_L |V| \qquad [20a]$$

$$D_T = \alpha_T |V| \qquad [20b]$$

Substituting these identities into Equation 19 yields

$$D_{xx} = D_L \frac{(V_x)^2}{|V|^2} + D_T \frac{(V_y)^2}{|V|^2} \qquad [21a]$$

$$D_{yy} = D_T \frac{(V_x)^2}{|V|^2} + D_L \frac{(V_y)^2}{|V|^2} \qquad [21b]$$

$$D_{xy} = D_{yx} = (D_L - D_T) \frac{V_x V_y}{|V|^2} \qquad [21c]$$

Equations 18 and 21 are the main equations used in the transport and dispersion of a nonreactive solute in a porous media.

List of Assumptions. Several assumptions were made in the formation of the equations used in this model. Since these assumptions significantly limit

how well the model depicts the conditions of Puna, it is important to review them.

1. Groundwater flow and solute transport are transient three-dimensional problems. For simplicitly this study will be confined to a two-dimensional case. The model consists of a horizontal layer of varying thickness. Vertical variations of head and concentrations are considered to be negligible and other parameters are also averaged in the vertical direction. The main problem with this assumption is the vertical averaging of concentration, temperature, and permeability. Unfortunately, the majority of measurements for the wells are confined to surface samples. But examination of temperature profiles indicate that temperatures remain relatively constant with depth except in GTW-3 (2982-01) and Malama-ki (2783-01). It is probable that thermal density inversions may also occur in these wells. The permeabilities are known to decrease with depth. Unfortunately, no good estimate of this parameter exists in relation to depth.

The model will also assume that the system is in steady state with respect to head. This means that the heads are assumed to be constant over time.

2. Darcy's law is assumed to be valid and the hydraulic heads are considered to be the only significant driving mechanism of the flow. The major problem with this assumption is that it ignores the effect of the existing temperature gradient. Some temperature effects have been incorporated in the value of the dynamic viscosity. But heat convection and density effects have not been considered.

3. Porosity and intrinsic permeabilities are considered constant over time. The principal directions of the permeabilities are assumed to be aligned with the coordinate axes of the model and the aquifer is considered to be isotropic with respect to permeability. The alignment of dikes, faults, and fractures suggest that the permeability of the rift zone is anisotropic.

Porosity is assumed to be uniform in space

4. The Ghyben-Herzberg lens is assumed to exist throughout the entire area of study. The existence of the basal lens within the rift zone is questionable. Macdonald (1977) suggests that no basal lens exists. However, this assumption is necessary to get an estimate of the saturated thickness.

5. No reactions occur that affect the concentrations of the solute, the fluid properties, or the aquifer properties. This is a valid assumption since chloride is the only chemical species considered and it is relatively unreactive.

6. Advection and dispersion are the only major components of the total dispersive flux. This assumes that ionic and molecular diffusion are negligible.

7. The aquifer is considered isotropic with respect to the coefficients of longitudinal and transverse dispersivities.

8. In the simulations, the injection is assumed to occur directly at the surface of the water table. However at HGP-A, the effluent is allowed to seep to the groundwater through settlement ponds. Any reduction in the effluent concentration is not considered in this study.

Numerical Solution and Grid System

Flow Equation. The flow equation as written in Equation 12 is difficult to solve because of its nonlinear form. If a linear form for the equation can be derived, the solution can be easily found using finite difference techniques. Equation 12 can be linearized by letting

$$T_{ij} = K_{ij} b_{n-1} \qquad [22]$$

where

T_{ij} is the principal component of the transmissivity tensor (L^2/t); and

n is the iteration index (Bear, 1979).

Substituting the transmissivity relationship into Equation 12 gives

$$\frac{\partial}{\partial x_i}\left(T_{ij}\frac{\partial h}{\partial x_j}\right) = Sy\frac{\partial h}{\partial t} + W(x,y,t) \qquad [23]$$

The solution to the flow equation as written in Equation 23 requires the application of finite difference methods. The finite difference approach requires that the area of interest be divided into rectangular blocks, in which the properties are considered to be uniform. Therefore, a nodal point in the center of the block can be assigned the properties of the entire block. The continuous derivatives in Equation 23 are estimated as the quotient-difference between nodal points. Using the block-centered, implicit fintie difference scheme, as outlined by Trescott et al. (1976), Equation 23 can be approximated by

$$\frac{1}{\Delta x_j}\left[\left(T_{xx}\frac{\partial h}{\partial x}\right)_{i,j+1/2} - \left(T_{yy}\frac{\partial h}{\partial x}\right)_{i,j-1/2}\right.$$

$$+ \frac{1}{\Delta y_i} \left[\left(T_{yy} \frac{\partial h}{\partial y} \right)_{i+1/2,j} - \left(T_{xx} \frac{\partial h}{\partial y} \right)_{i-1/2,j} \right.$$

$$= \frac{Sy}{\Delta t} (h_{i,j,k} - h_{i,j,k-1}) + W_{i,j,k} \qquad [24]$$

in which

x is the space increment in the x direction for column j (L);

y is the space increment in the y direction for row i (L);

t is the time increment (t)

i is the index in the y direction;

j is the index in the x direction;

k is the time index.

Using finite difference approximations for the transmissivity and the heads, Equation 23 can be expressed as

$$F_{ij} (h_{i,j+1} - h_{i,j}) - D_{ij} (h_{i,j} - h_{i,j-1})$$
$$+ H_{ij} (h_{i+1,j} - h_{i,j}) - B_{ij} (h_{i,j} - h_{i-1,j})$$
$$= \frac{Sy}{\Delta t} (h_{i,j,k} - h_{i,j,k-1}) + W_{i,j,k} \qquad [25a]$$

in which

$$B_{ij} = \frac{\frac{2T_{yy[i,j]}T_{yy[i-1,j]}}{T_{yy[i,j]}y_{i-1} + T_{yy[i-1,j]}y_i}}{\Delta y_i} \qquad [25b]$$

$$D_{ij} = \frac{\frac{2T_{xx[i,j]}T_{xx[i,j-1]}}{T_{xx[i,j]}x_{j-1} + T_{xx[i,j-1]}x_j}}{\Delta x_j} \qquad [25c]$$

$$F_{ij} = \frac{\dfrac{2T_{xx[i,j]}T_{xx[i,j+1]}}{T_{xx[i,j]}x_{j+1} + T_{xx[i,j+1]}x_j}}{\Delta x_j} \qquad [25c]$$

$$H_{ij} = \frac{\dfrac{2T_{yy[i+1,j]}T_{yy[i,j]}}{T_{yy[i,j]}y_{i+1} + T_{yy[i+1,j]}y_i}}{\Delta y_i} \qquad [25d]$$

Rewriting Equation 25 so all the unknowns are on the left-hand side gives

$$Bh_{i-1} + Dh_{j-1} + Eh + Fh_{j+1} + Hh_{i+1} = Q \qquad [26]$$

in which

$$E = -\left(B + D + H + \frac{Sy}{\Delta t}\right)$$

$$Q = \frac{Sy}{\Delta t} h_{k-1} + W$$

Equation 25 will be solved using the iterative alternating-direction implicit (IADI) procedure as described by Trescott et al. (1976). The IADI method uses two sets of equations for each iteration by using two time steps. In the first, the head values along a column are expressed explicitly in terms of known values from the previous time step (n-1) and the values along rows are expressed implicitly at the n-1/2 time step. The equation for this first step can be expressed as

$$Dh_{j-1} + E_r h_j + F_{j+1} = Q_r \qquad j = 1, 2, \ldots N_x \qquad [27a]$$

in which

$$E_r = -\left(D + F + \frac{Sy}{\Delta t} + M_\ell\right)$$

$$Q_r = - Bh_{i-1}^{n-1} + (B + H - M_\ell)h^{n-1} - Hh_{i+1}^{n-1} - \frac{Sy}{\Delta t} h_{k-1} + W$$

where

M_ℓ is the iteration parameter; and

ℓ is the iteration parameter index.

With the results from the first time step, head values along the columns are considered implicitly and those along the rows are explicitly written as

$$Bh_{i-1}^{n} + E_c h^{n} + Hh_{i+1}^{n} = Q_c \qquad i = 1, 2, \ldots N_y \qquad [27b]$$

in which

$$E_c = - (B + H + \frac{Sy}{\Delta t} + M_\ell)$$

$$Q_c = - Dh_{j-1}^{n-1/2} + (D + F + M)h^{n-1/2} - Fh_{j+1}^{n-1/2} - \frac{Sy}{\Delta t} h_{k-1} + W$$

Each set of equations results in a tridiagonal matrix which is then solved using the Thomas algorithm. The process is continued until the heads meet the convergence criterion. In this study, the convergence criterion for the iteration will be a cummulative error of 0.001 meters. This means that the sum of the differences between the calculated heads from row and column iterations must sum to less than 0.001 meters.

Transport Equation. The transport equation as written in Equation 18 will be solved by the method of characteristics (MOC) as outlined by Konikow and Bredehoeft (1978). In general, the MOC formulates an equivalent set of differential equations based on a moving reference system. Reference points are moved some distance depending on the velocity and the length of the time increment. Then, the concentrations for each cell are calculated from the points within the area. Once the convective effects have been calculated, the

remaining variables are computed using finite difference approximations and matrix calculations (Faust and Mercer, 1980).

The time period over which the transport will be analyzed will be 25 years as used by Liu et al. (1984). After this time, the system will be assumed to be in a steady state.

The Grid System. A rectangular node centered grid was overlain on a 1:100,000 scale USGS topographic map. For convenience the grid cells were chosen to be two kilometers by two kilometers. The study area consists of ten cells along the horizontal axis and six cells in the vertical direction. The no-flow boundary surrounds the area as required by the model.

Figure 14 also shows the location of the pumping well and the designation of the rift zone. The discharge of the Airport well (3081-01) will be approximated by four discharge cells symbolized by the W because the well is located near the intersection of the four blocks. The east rift zone will be approximated by the shaded area. The mathematical boundary of the rift was determined by locating the blocks in which at least half of the block lay within the physical boundary of the rift. Unfortunately, the model does not allow for different-sized blocks which would fit the physical boundaries better.

Boundary and Initial Conditions

Two major types of boundary conditions are often introduced in groundwater modeling: prescribed head boundaries and prescribed flow boundaries. Due to the lack of information of groundwater flux thru the area, only prescribed head boundaries were used. Using a prescribed flow boundary

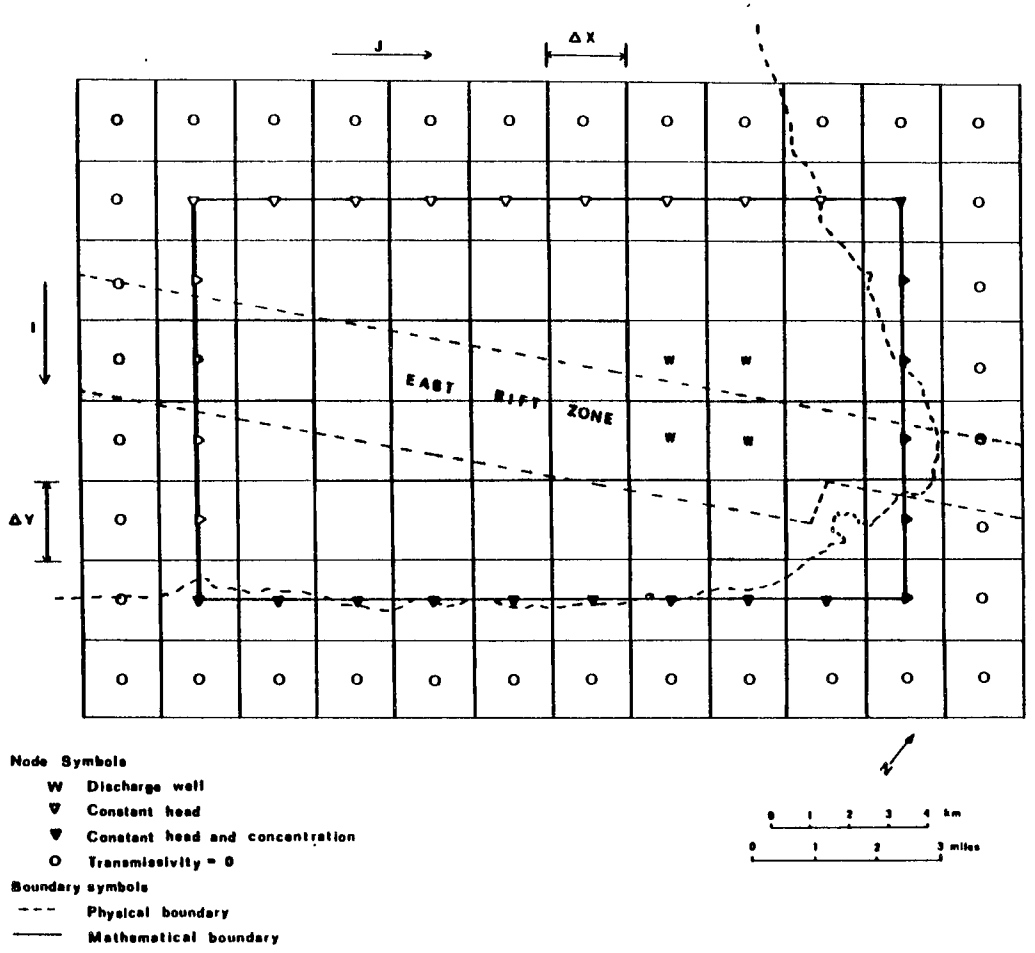

Figure 14. Grid System

would imply a constant gradient along the entire length of the boundary and that the direction of flow is perpendicular to the boundary which may not be true.

The study area was positioned such that the coasts could be designated as zero head and constant concentration boundaries. The other boundaries were located where the best well control exists, avoiding any perched water bodies. The heads along these boundaries were determined by constructing an equipotential map of the study area using head data from wells.

In this study, initial heads will be assigned to each nodal point. Hence, it will be assumed that the freshwater lens already exists in its present form. All chloride concentrations will be initialized at zero except along the coasts where the chloride concentrations are 100% of that for ocean water. The head and chloride distributions will be calibrated using well data.

CHAPTER IV

RESULTS

Calibration

Flow Equation. The flow portion of the model determines the hydraulic heads as governed by the flow equation (Equation 1). To simulate the flow of groundwater through the area, values for recharge from precipitaion, well discharge, water temperature, and intrinsic permeability were assigned to each nodal point. From these initial conditions, the hydraulic conductivity, the saturated thickness, and the transmissivity for each nodal point were calculated by Equations 5, 11, and 22 respectively. A set of simultaneous equations in the form of Equation 25 was obtained and solved by the IADI method. The iteration continued until the heads converged.

The flow submodel was calibrated by comparing the calculated heads to the heads measured in the Puna wells. The calculated heads were fit by varying two parameters: the prescribed heads of the inland boundaries and the intrinsic permeabilities. The heads that define the inland boundaries were obtained from an equipotential map prepared from well water levels. However, due to the limited number of wells in the area, the prescribed head values were very poorly constrained. Changing the head values caused local variations but did not radically alter the total head distribution. This method of calibration was very effective for the blocks near the boundaries.

By varying the intrinsic permeabilities, a reasonable estimate of the intrinsic permeabilities was obtained and the effects of permeabilities on groundwater flow through the rift system could be examined. A regional permeability was assigned to the area, and a rift system of lower permeability

was emplaced within it. Then the heads were calculated. The permeability assigned to the non-rift area was 4.9×10^{-5} cm^2 (5000 darcys), and in the rift zone, between 9.8×10^{-8} (10 darcys) and 4.9×10^{-6} cm^2 (500 darcys) were used.

The effectiveness of the rift zone as a barrier to groundwater flow is highly dependent on the permeabilities assigned to the rift and non-rift areas (see Figures 15a and 15b). As can be seen in Figure 15a where the permeability contrast between non-rift and rift material is 5000 to 10, the rift acts as an effective flow barrier and heads on the north side of the rift are significantly higher than on the south side. In Figure 15b where the permeability contrast is only 5000 to 500 the rift acts as a much less effective barrier.

In actuality, the assigned values for permeability used in Figure 15a computed heads in and near the rift zone that were much greater than those actually observed in wells. Increasing the rift permeabilities resulted in better fitting heads within the rift, but caused the computed heads south of the rift to become too high (Figure 15b). (It should be noted that because well 3081-02 (Kapoho Shaft) is thought to be perched and not basal water, it was not considered in the calibration). One solution to this problem was to increase the permeabilities of the non-rift area to 7.4×10^{-5} cm^2 (7500 darcys). This caused the heads to decrease slightly as shown in Figure 15c, however, the resultant calculated hydraulic conductivities ranged between 6558 to 11,405 m/d, which seemed unreasonably large. Another solution to this problem was to allow the permeabilities in the rift zone to change where the buttressing effect of Mauna Loa dies out. Several combinations were tried.

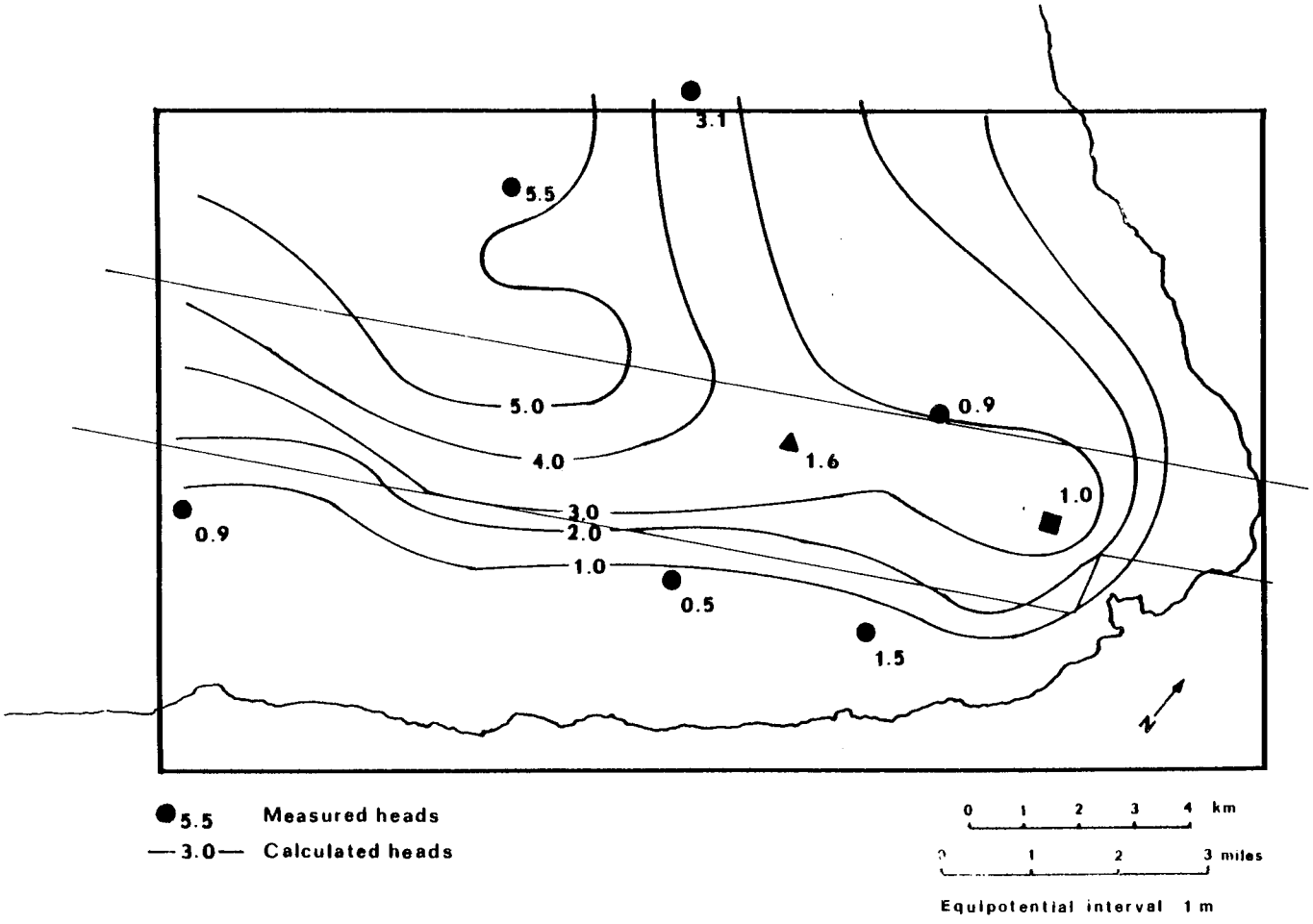

Figure 15a. Calculated Head Distribution
$k_{non-rift} = 4.9 \times 10^{-5}$ cm^2
$k_{rift} = 9.8 \times 10^{-8}$ cm^2

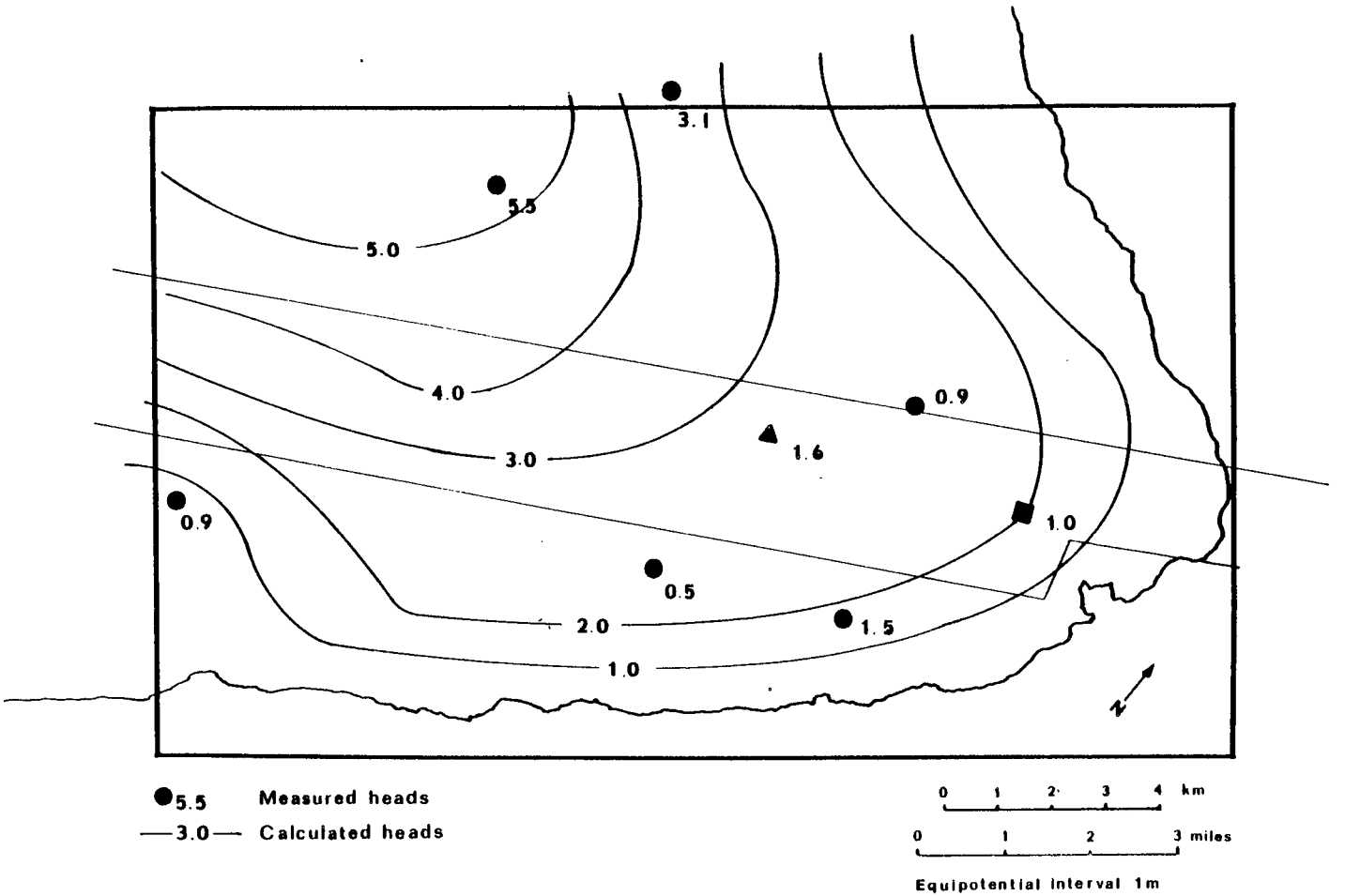

Figure 15b. Calculated Head Distribution
$k_{non-rift} = 4.9 \times 10^{-5}$ cm^2
$k_{rift} = 4.9 \times 10^{-6}$ cm^2

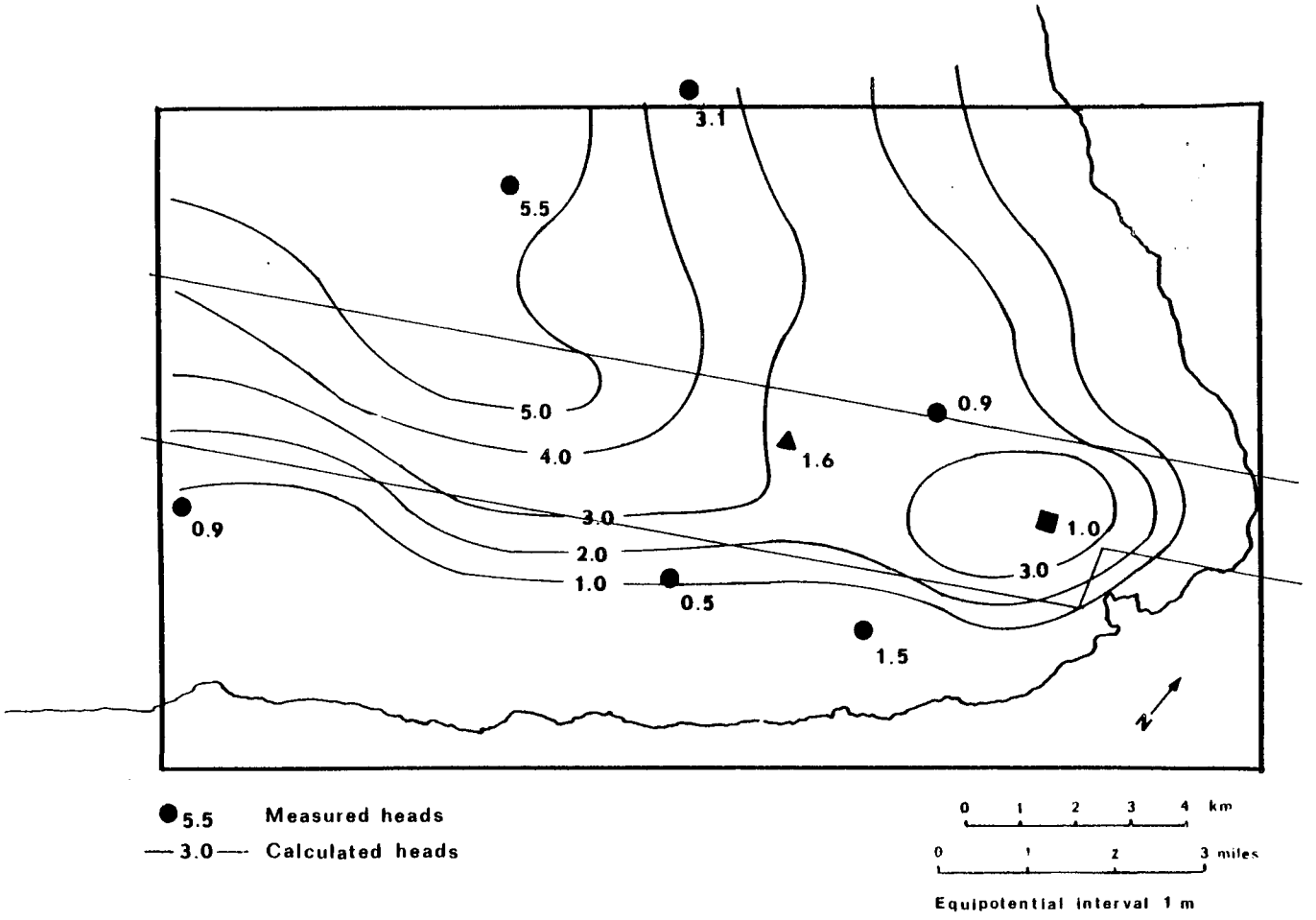

Figure 15c. Calculated Head Distribution
$k_{non-rift} = 7.4 \times 10^{-4}$ cm^2
$k_{rift} = 9.8 \times 10^{-8}$ cm^2

The best combination shown in Figure 15d, assigns the permeabilities of the upper portion of the rift to be 9.8×10^{-8} cm^2 (10 darcies) and 9.8×10^{-6} cm^2 (1000 darcys) in the lower section. Some problems still exist in the calibration of the heads south of the rift, especially with well 2783-01 (Allison), perhaps because the changes in the permeabilities along the rift are actually more graduated than suggested in Figure 15d (see Figure 15e). Since the heads estimated using the two permeability rift fits the data reasonably well, however, this version was selected.

Transport Equation. The distribution of chlorides was determined by using the method of characteristics to solve the diffusion equation (Equation 18). The assigned dispersivities and the velocities were used to calculate the dispersion coefficients, D, for each node (Equations 20 and 21). The dispersion was allowed to continue for 25 years.

The transport submodel was calibrated by introducing dispersivity values, β, and comparing the computed chloride distribution to the values measured in wells. A range of dispersivity values from 7.6 meters to 1000 meters was used (Figures 16a and 16b respectively). For β = 1000 m the fit is reasonably good except where temperatures are abnormally high such as wells 2982-01 (GTW-3) and 2783-01 (Malama-ki) (Figure 16b). The calculated chloride concentrations for the two high temperature wells were too low.

In this model it was assumed that the only source of chlorides is from the ocean, thus vertical mixing was not considered. Since the amount of vertical mixing also increases as temperature increasese, a function that incorporated the temperature dependent vertical mixing was used. From the results of previous simulations, an exponential relationship between

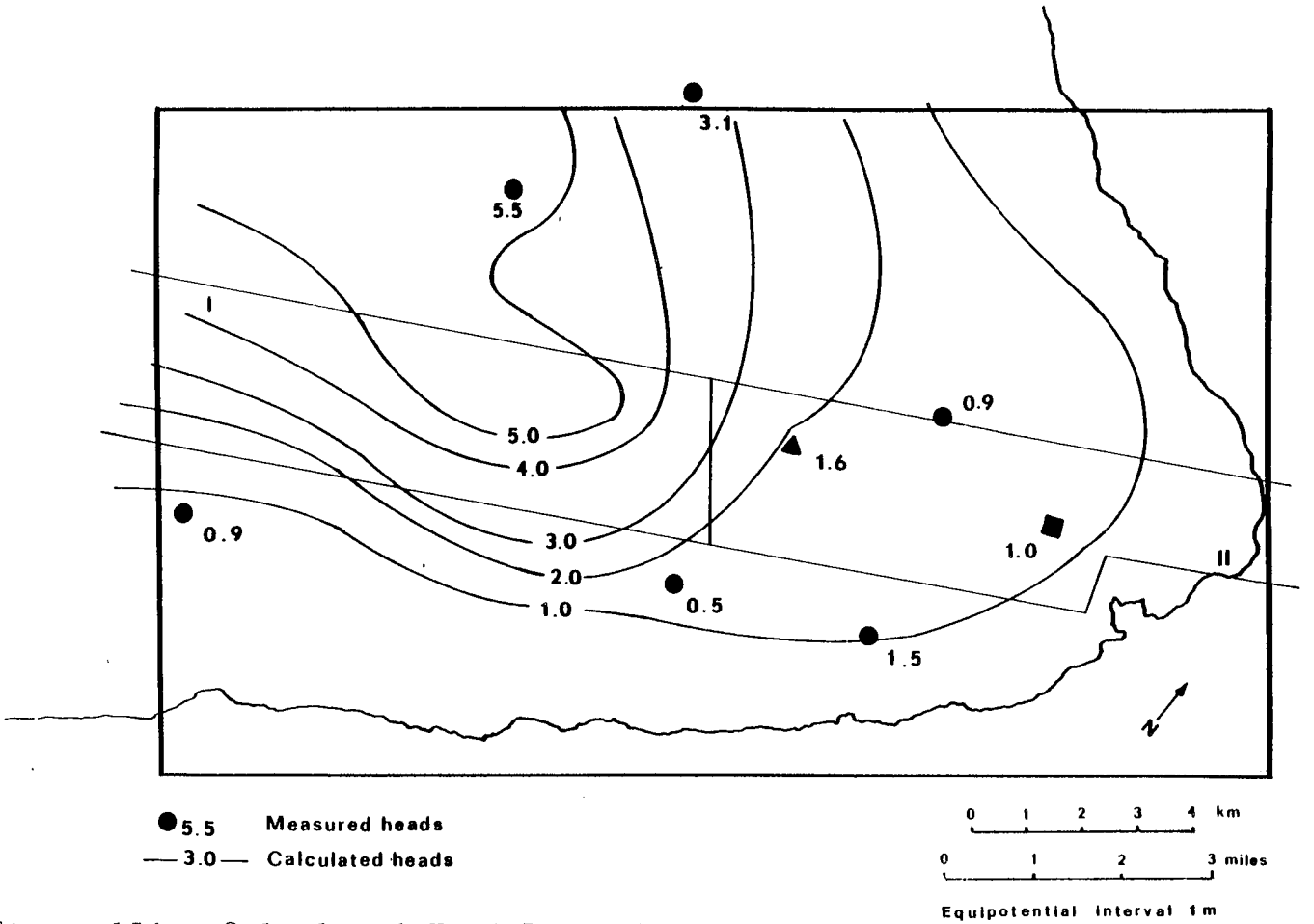

Figure 15d. Calculated Head Distribution

$k_{non\text{-}rift} = 4.9 \times 10^{-5}$ cm^2

$k_{rift\text{-}1} = 9.8 \times 10^{-8}$ cm^2

$k_{rift\text{-}11} = 9.8 \times 10^{-6}$ cm^2

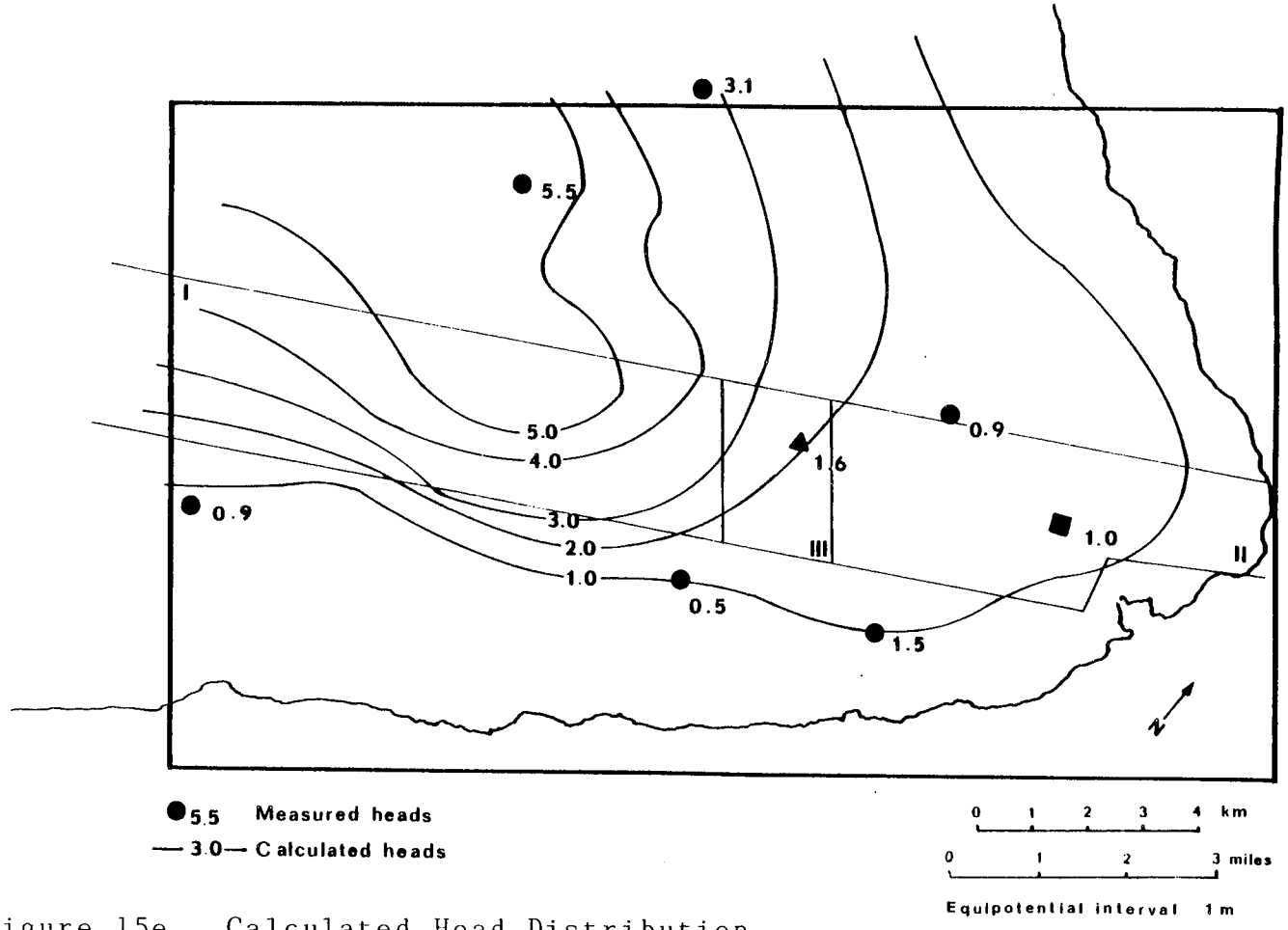

Figure 15e. Calculated Head Distribution

$k_{non\text{-}rift} = 4.9 \times 10^{-5}$ cm^2

$k_{rift\text{-}1}$ 9.8×10^{-8} cm^2

$k_{rift\text{-}11}$ 9.8×10^{-6} cm^2

$k_{rift\text{-}111}$ 9.8×10^{-7} cm^2

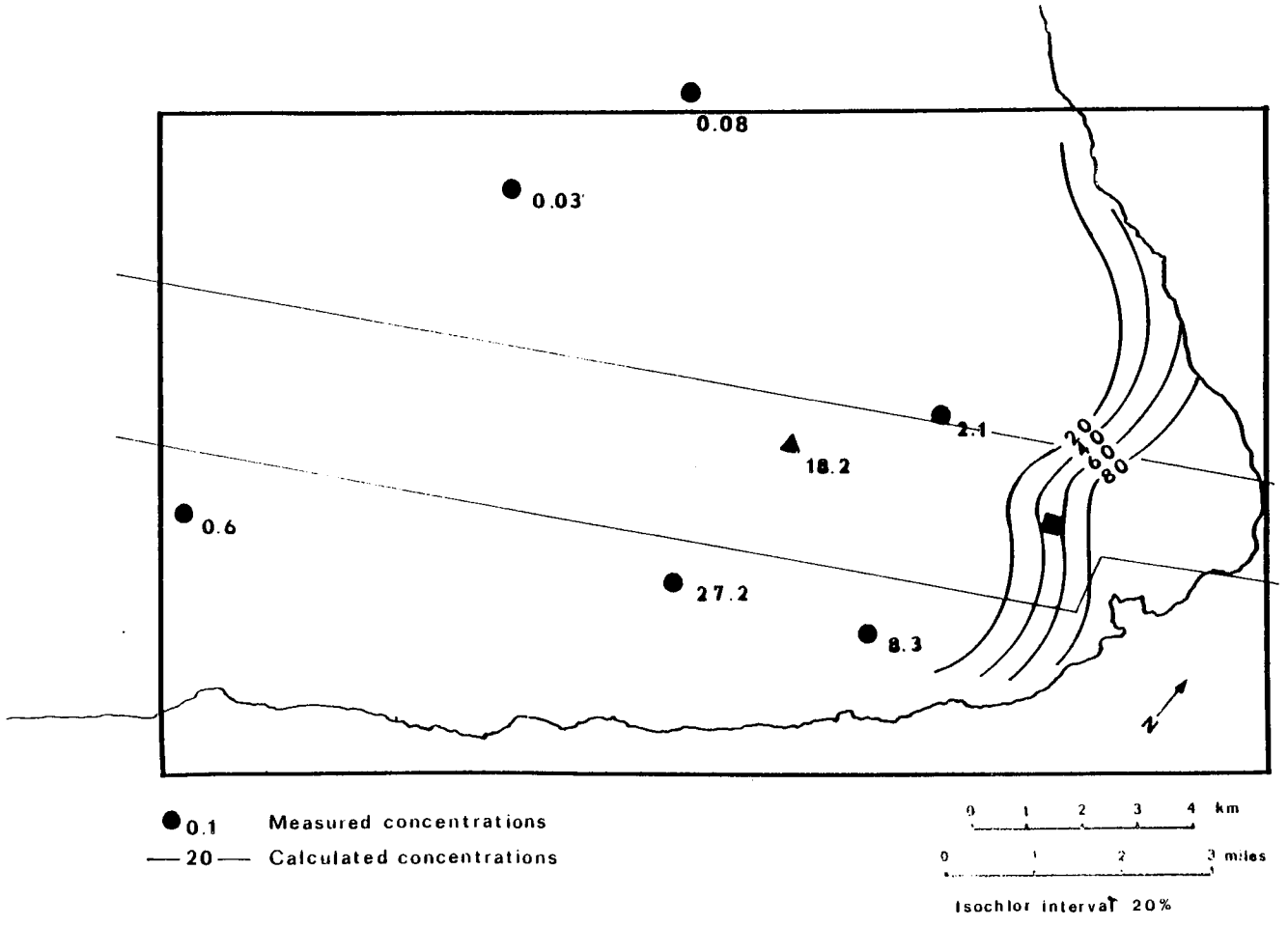

Figure 16a. Calculated Chloride Distribution
β = 7.6 m

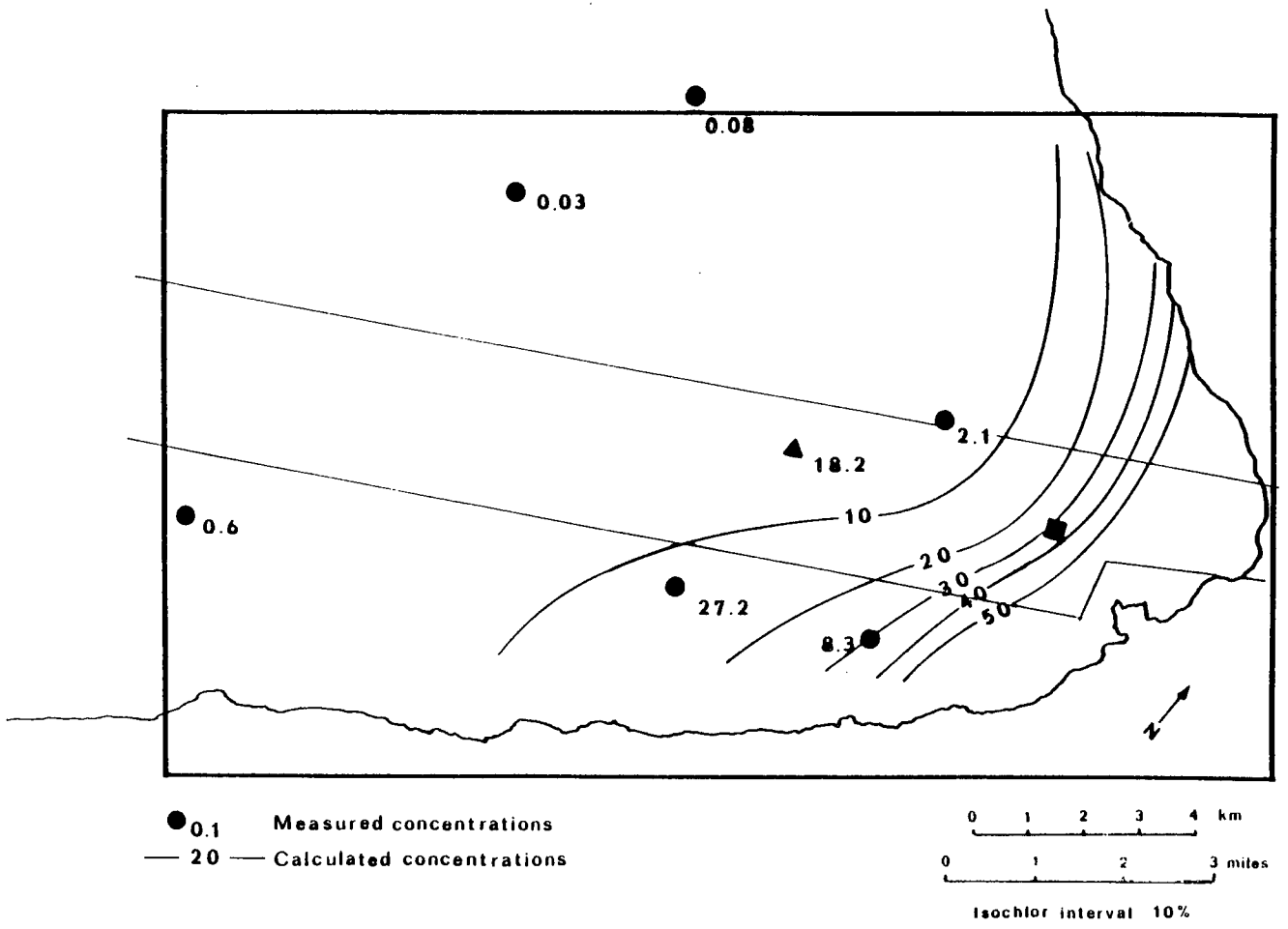

Figure 16b. Calculated Chloride Distribution
β = 1000 m

dispersivity and temperature was developed. The function

$$\beta = 10668.26 \times EXP[-0.0392 + (100 - T)] \quad [27]$$

gave a chloride distribution most resembling the observed data (Figure 16c). The dispersivity values ranged from 500 meters for normal temperatures (T = 22 °C) to 4000.9 meters for temperatures of 75 ° C. However, some discrepancies still exist, especially for the high temperature wells where the calculated concentrations are still too low. The high chloride concentration calculated for the Allison well (2881-01) can be attributed to boundary affects. Problems in the calibration may be due to the high dispersivities used. If lower dispersivities were used, for example where β = 100 m for normal temperatures, it would take about three minutes of computer time for steady state to be reached, thus making it very expensive. Since the general trends are similar, the use of smaller values of dispersivities could not be justified due to the high cost.

Simulations

Once the model was calibrated, the effects of seepage of geothermal effluent into the groundwater system were examined by injecting geothermal effluent of a specified concentration into the aquifer and calculating the chloride distribution at the end of a 25 year period. The initial conditions of the aquifer are those derived from the calibration of the model. The nodal point closest to the location of HGP-A was selected as the point of injection. An injection rate of 0.0084 m^3/s (800 gph) was suggested by D. Thomas (personal communication, 1984). The chloride concentration of the geothermal effluent has increased since 1976 from 1200 ppm to between 10,000 and 11,000

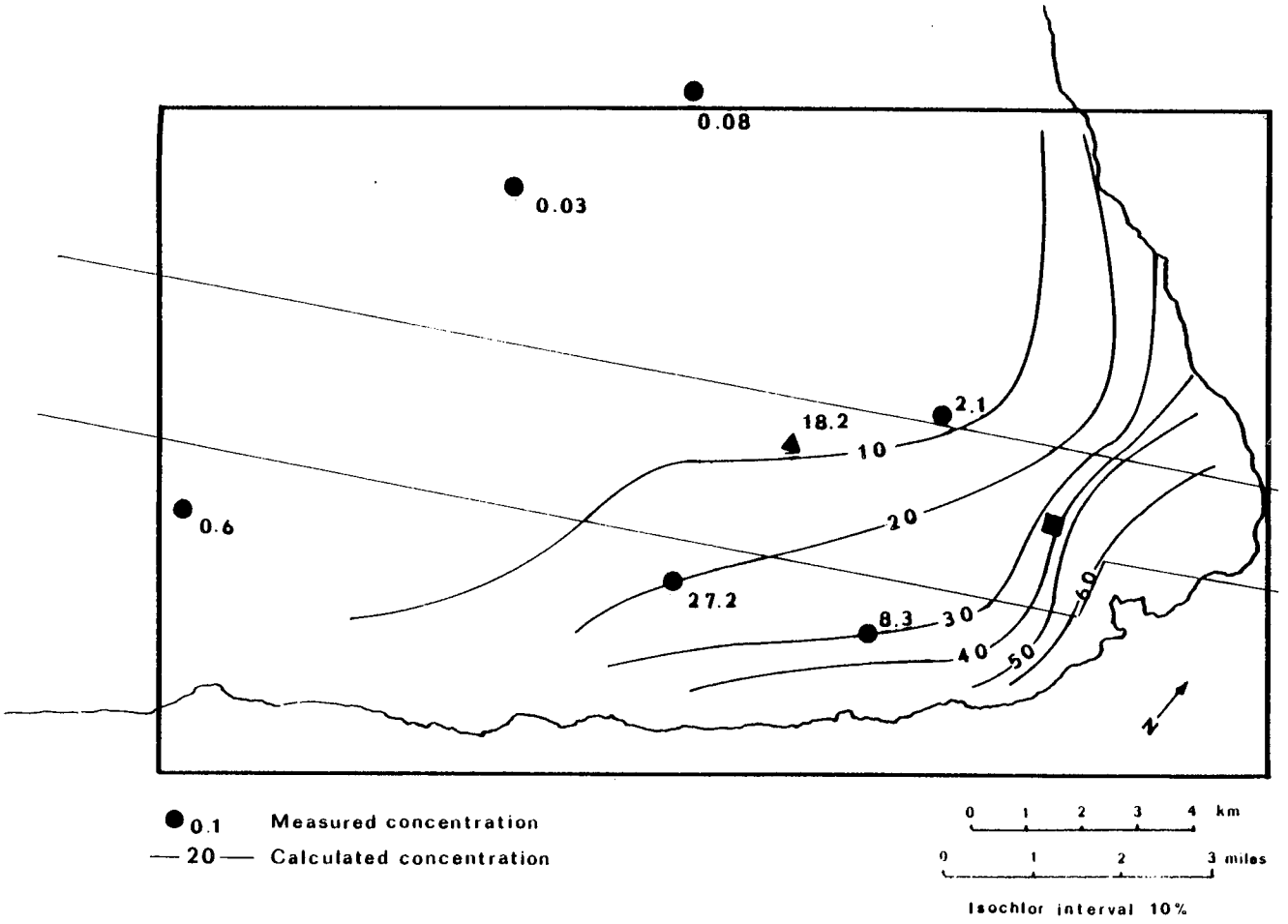

Figure 16c. Calculated Chloride Distribution
$\beta = 10668.26 \exp(-0.0392 \times (100 - T))$

ppm at present (Table 5). Therefore, three simulations were made: 1200 ppm representing the years from 1976 to 1981, 3778.5 ppm for the years 1982 to 1983, and 10,000 ppm for the present and possible future.

In the first simulation, an effluent with a chloride concentration of 1200 ppm or about 6.38% of the salinity of seawater was injected. Figure 17a shows the calculated distribution of chlorides after 25 years. As expected, the isochlors shifted slightly and the overall chloride distribution did not change significantly. The changes in concentration due to the injection of the effluent are shown in Figure 17b. After 25 years, the increase in salinity due to the injection of the effluent is elongated to the northeast as would be expected by the gradients. The largest increase, 0.40% or about 75 ppm, was found at the point of injection, decreasing to 0.1% (about 18.8 ppm) five kilometers from the well.

An effluent concentration of 3778.5 ppm (about 20.01% of the salinity of seawater) was used in the second simulation (Figure 18a). Except for the increase in chloride concentration, the overall chloride distribution pattern did not change significantly after 25 years of injection. The changes in concentration due to the injection are shown in Figure 18b. As expected, the area of influence of the injection was greatly expanded. The chloride concentration at the injection well was 1.66% or about 200 ppm and the concentrations decreased to 0.1% (18.8 ppm) by about seven kilometers northeast of the well.

The final simulation injected an effluent with 10,500 ppm chloride or about 55.85% of the salinity of seawater (Figure 19a). Unlike the previous simulations, the injection greatly altered the overall chloride distribution.

Figure 17a. Calculated Chloride Distribution
Effluent Concentration = 6.4% (1200 ppm)

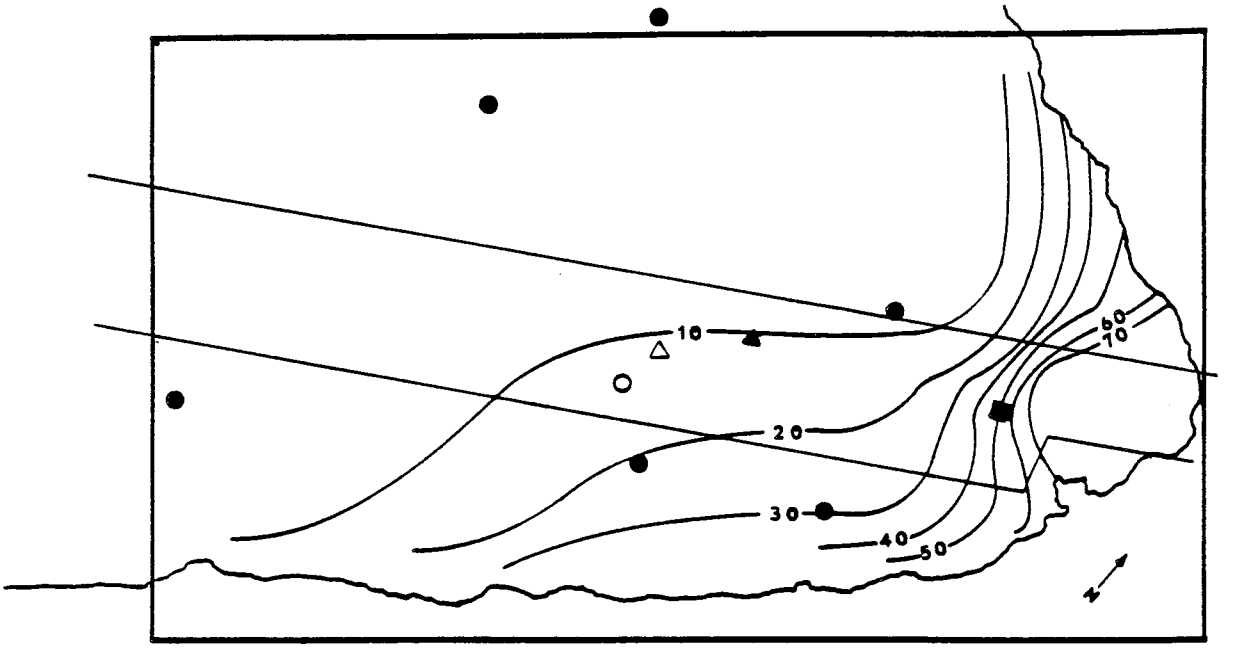

Figure 17b. Changes in Concentration

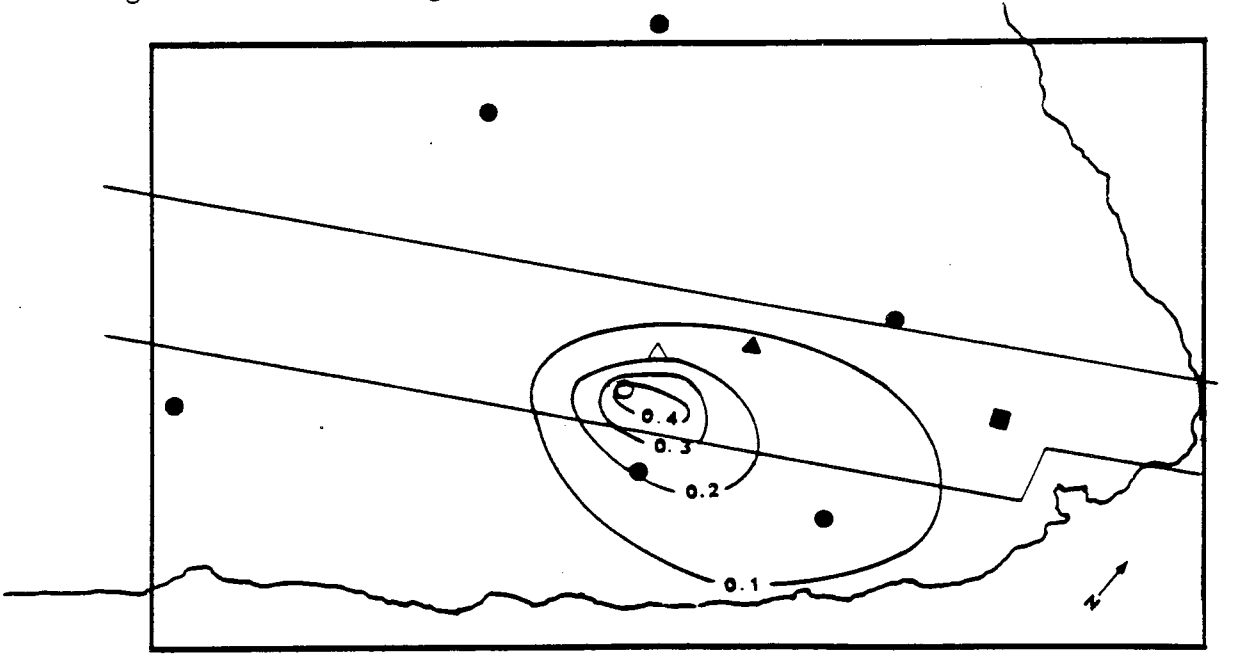

O Injection well

0 1 2 3 4 km
0 1 2 3 miles
Isochlor interval 0.1%

Figure 18a. Calculated Chloride Distribution
Effluent Concentration = 20.0% (3778.5 ppm)

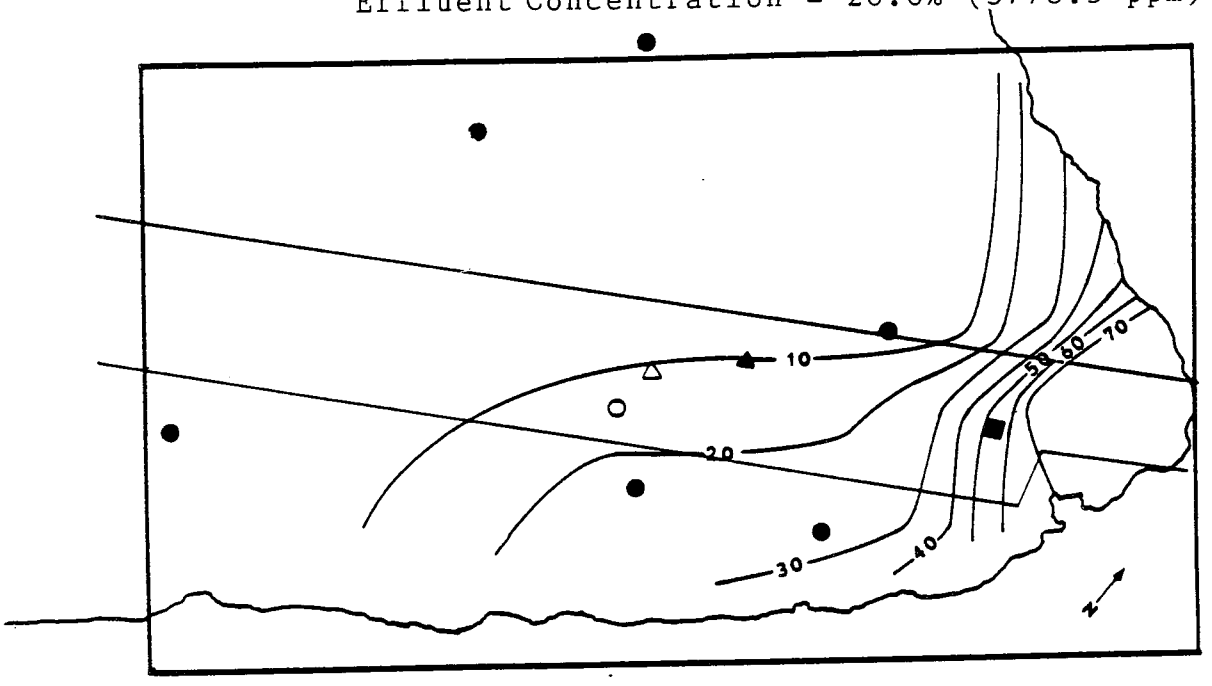

Figure 18b. Changes in Concentration

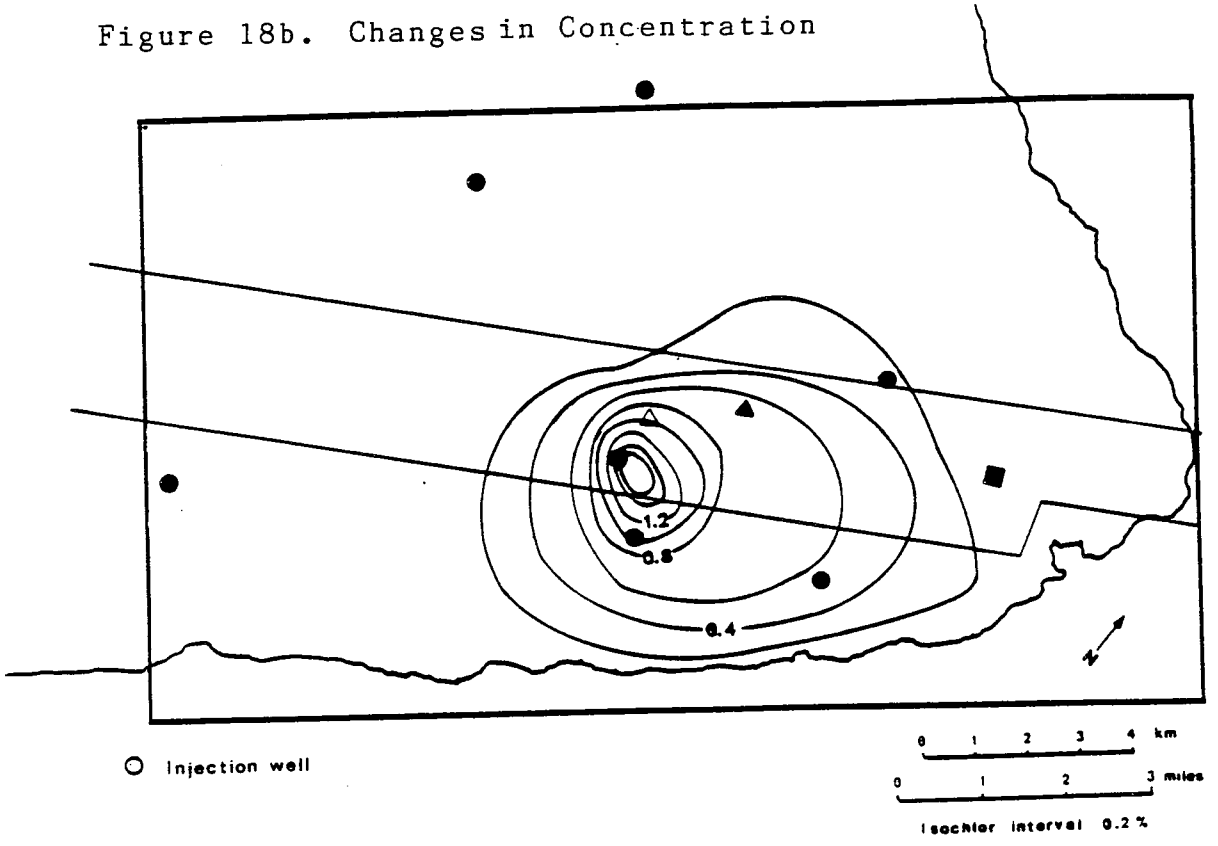

Figure 19a. Calculated Chloride Distribution
Effluent Concentration = 55.9% (10,500 ppm)

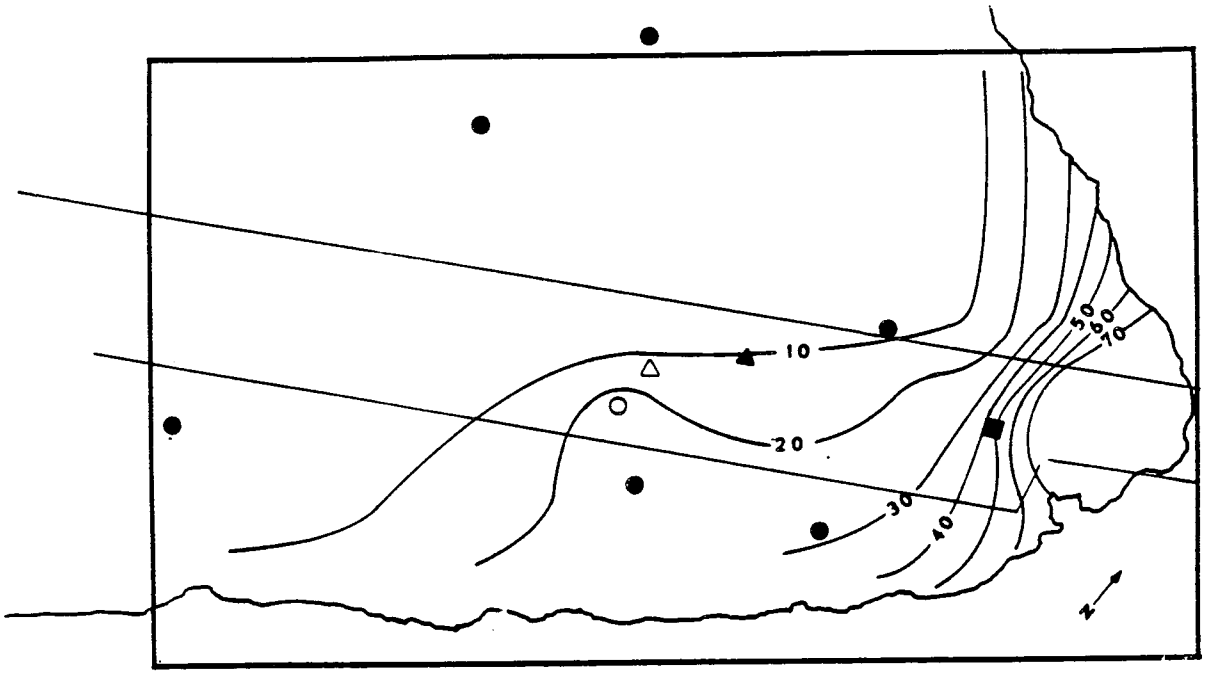

Figure 19b. Changes in Concentration

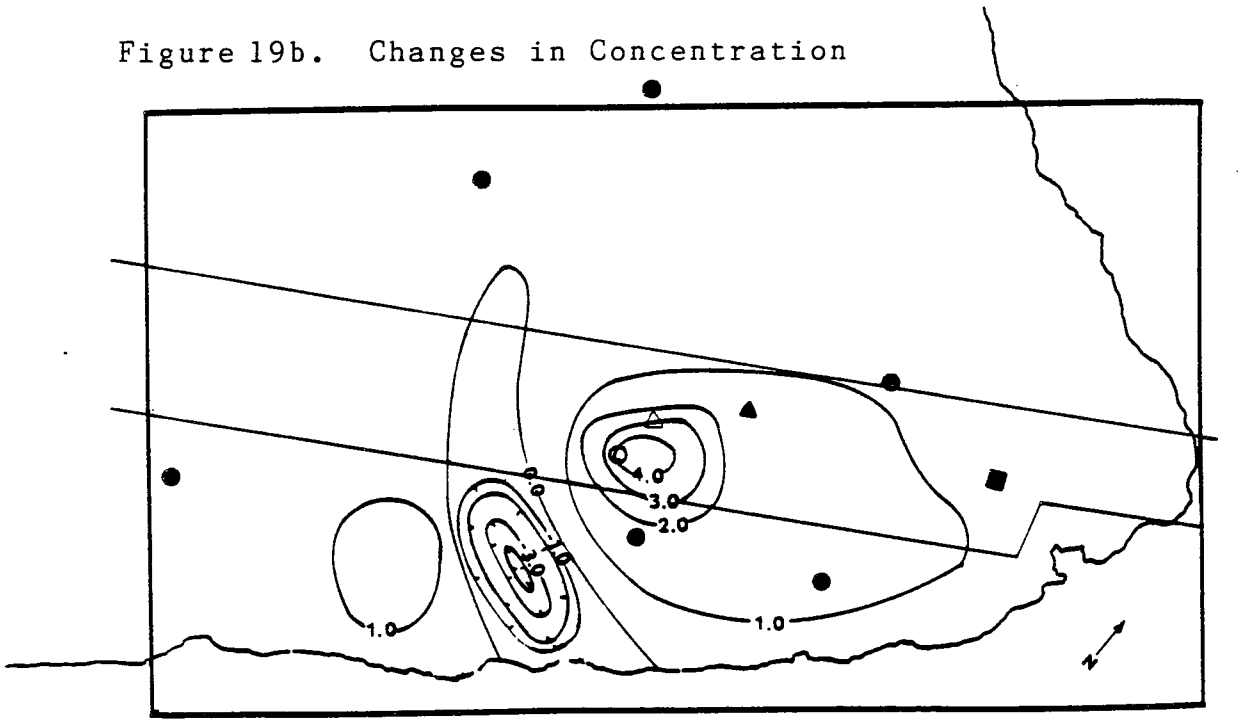

The effects of the injection were calculated by removing the undisturbed chloride distribution (Figure 19b). It seems that the injection of such a high concentration caused a chemical sink to form as shown by the negative numbers. This may be because the model has not reached an equilibrium after 25 years; the concentrations were still oscillating at the end of the period. Still, as a result of the injection, the chloride concentrations have increased significantly. The largest increase of 4.0% or about 754 ppm was calculated at the injection well, decreasing to 0.1% by about 7.5 kilometers northeast of the well. This large area of influence and the large increase in chloride concentration is important since it will determine if the water is potable.

Presentation of Results

The calibration of the model has given some insights into the possible mechanisms controlling the hydrology of Puna. The east rift zone of Kilauea plays an important role in the groundwater flow through Puna. The effectiveness of the east rift zone as a barrier is a direct function of its permeability. The results of the model indicate that the rift zone consists of two or possibly more permeabilities. The upper portion of the rift was found to have intrinsic permeabilities of 9.6×10^{-8} cm^2 (10 darcys) while the lower section has permeabilities of 9.8×10^{-6} cm^2 (1000 darcys). This seems reasonable when considering the distance from the source magma and the buttressing effect of Mauna Loa. Since the lower section of the rift is farther from the source and no longer confined by Mauna Loa, the density of dikes may decrease allowing the permeabilities to increase. It is surprising

however, that the permeabilities of the lower portion are nearly as high as that of the non-rift areas (4.5×10^{-5} cm^2 or 5000 darcys).

The hydraulic conductivity is another measure of the ease of flow through a media. The hydraulic conductivities calculated by the model ranged between 4337.3 to 8277.1 m/day for the non-rift areas, between 17.8 and 32.4 m/day for the upper section of the rift, and 881.0 to 2350.1 m/day for the lower portion of the rift. The hydraulic conductivities for the non-rift areas are very high for Hawaiian basalts. Williams and Soroos (1973) found an average conductivity of 282 m/day (925 ft/day) using pump test analysis for wells on Oahu, Molokai and Maui. Other studies estimated a range of hydraulic conductivities between 305 m/day to 4000 m/d (Kanehiro and Peterson, 1977, Liu et al., 1983, and Imada, 1982). The high hydraulic conductivities suggested for the east rift zone may be due to the high basal water temperatures measured in Puna. The dynamic viscosities which are a function of temperature (Equation 6) ranged from 9.55×10^{-3} g/cm/s at 22 C to 3.78×10^{-3} g/cm/s at 75°C. Since the hydraulic conductivities are inversely proportional to the dynamic viscosities, this caused the conductivity values to be about two times larger than expected.

A water budget was calculated by the model. Of a recharge from precipitation of about 2.206×10^8 m^3/yr (about 160 MGD), approximately 2.071×10^8 m^3/yr (about 150 MGD) of water discharges into the ocean. After removing pumpage of about 2.16×10^4 m^3/yr (about 0.02 MGD), about 1.95×10^7 m^3/yr (about 10 MGD) or about 8.9% of the recharge remains unaccounted for. The discrepancy may be due to the assumption that the permeabilities are isotropic. This assumption restricts the amount of water that flows through

as well as across the rift. If instead the system was assumed to be anisotropic with respect to permeability as suggested by the trends of the dikes and fissures, it would allow large quantities of water to flow through the rift to the ocean. Another reason could be leakage into separate deep reservoirs in the rift zone such as the geothermal reservoir tapped by HGP-A.

The velocities of groundwater flow were also calculated by the flow submodel (Equation 15b). The magnitude and direction of the velocities are shown in Figure 20. The calculated velocities in the rift zone were extremely low, between 0.04 m/d and 3.34 m/d. The low velocities in the rift zone are due to the low intrinsic permeabilities assigned to the rift zone. The magnitude of the velocites of the non-rift areas were much higher than expected, ranging from about 1.6 to 16.7 m/d (5.3 to 54.5 ft/d) north of the rift to 0.7 to 27.7 m/d (2.2 to 90.9 ft/d) south of the rift. Davis and Yamanaga (1968) estimated the average velocity north of the rift to be between 1.2 to 2.4 m/d (4 to 8 ft/d) and 0.6 m/d (2 ft/d) south of the rift. The high velocities are the result of the high hydraulic conductivities estimated; since the velocity is directly proportional to the hydraulic conductivity. It was surprising that the velocities south of the rift are higher than those north of the rift, but this may be due to the high head gradients caused by the dike impoundment of water. Due to the small quantities of water which can flow across the rift, however, the flux through the area must be rather limited.

The transport submodel was calibrated by varying the value of the dispersivity. To incorporate the vertical mixing into the model, the dispersivities were calculated as a function of the temperature (Equation 27).

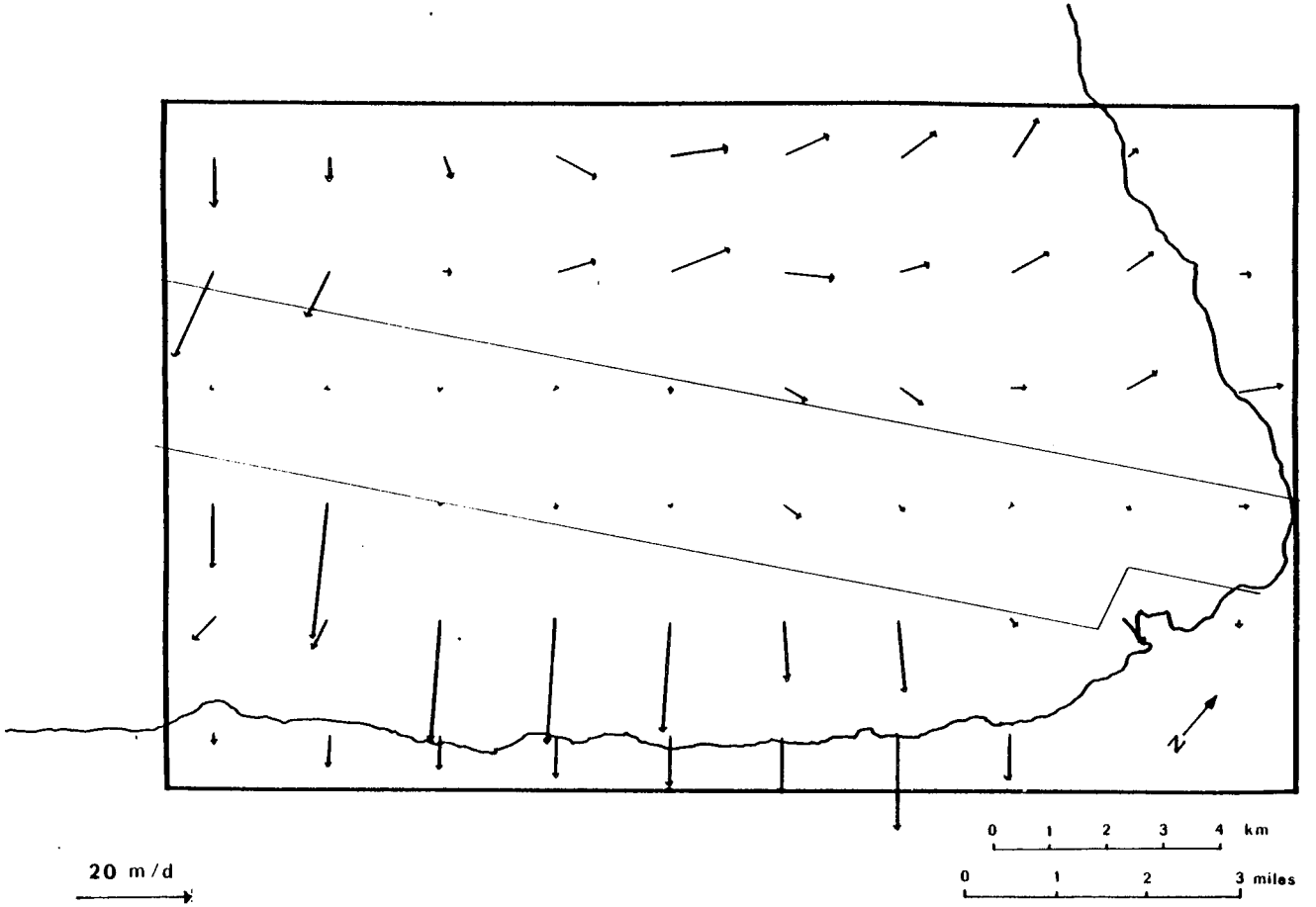

Figure 20. Calculated Velocities

The dispersivities were much larger than expected, ranging from 501.4 m for temperatures of 22°C to 4003.9 m for temperatures of 75°C. These values are much larger than the 0.76 m estimated by Liu et al (1983) for the Pearl Harbor aquifer for a number of reasons. First, the model used in this study is a horizontal plane while Liu et al. used a vertical cross-section. Therefore, the dispersivities are averaged in the vertical direction instead of in the horizontal direction and hence, it is incorrect to compare the dispersivity values from the two studies. Vertically averaged dispersivity values of up to 100 m have been used to simulate dispersion of contaminants in sandy aquifers (Freeze and Cherry, 1979). Since the permeabilities of the Hawaiian aquifers are much higher than that of sandy aquifers, it is likely that the dispersivities are also higher. Secondly, in areas of high temperatures the dispersivities must be high to include the additional input of chlorides due to vertical mixing. Finally, the dispersivity values at normal temperatures may actually be much lower than the values used, but the use of low dispersivities extended the time required to achieve steady state beyond 25 years, thus making computer simulations much more costly.

A major purpose of this study was to examine the effects of geothermal activity on the groundwater in Puna. Three simulations injecting between 1200 to 10,500 ppm were conducted. The results showed that the effects of the seepage of the effluent into the groundwater is highly dependent on the effluent concentration. If the concentrations were low (1200 or 3778.5 ppm), the increases in the chloride concentrations in the groundwater was not significant over 25 years. But, if the chloride concentration of the effluent was high (10,500 ppm), then water quality problems will occur after the 25

year period. It should be noted however, that the injection at the high concentration may have caused the model to become unstable or the model may have not reached steady state after 25 years.

To further check the validity of the injection phase of the modeling, the chloride concentrations from the simulations were compared to measured chloride concentrations for the year 1981. The average measured concentrations are given in Figure 21. As predicted, the major changes in salinity occured south of the rift and to the northeast of the HGP-A. Three major changes have occurred: GTW-3 (2982-01) showed an increase in chlorides of about 1514.7 ppm (8.2% of the salinity of seawater), Allison (2881-01) showed an increase of 601.3 ppm (3.3%) and Malama-ki (2783-01) showed a decrease of 1736.0 ppm (9.4%). The large increase at GTW-3 was much larger than anticipated from any of the simulations. This again may be due to the anisotropic nature of the rift system. If water flows through the rift, the effluent would also be transported down rift, resulting in higher chloride concentrations at GTW-3. Still, the effects of the injection over the short term was much larger than expected by any of the simulations.

A caveat is in order here. The measured chloride concentrations are greatly affected by several factors. The most important of these is recharge. As water recharges the aquifer, it flushes some of the chlorides out of the system, thereby lowering the concentration. The period of measurement was not long enough to remove all of these effects. Secondly, a question exists about steady state. The model assumed that a steady state condition was attained after 25 years. Yet problems still occurred in the last simulation (effluent concentration was 10,500). Moreover, the measured data was collected after

Figure 21a. Average Chloride Concentrations for 1981 in ppm, numbers in () are % salinity of seawater (Epp, personal communication)

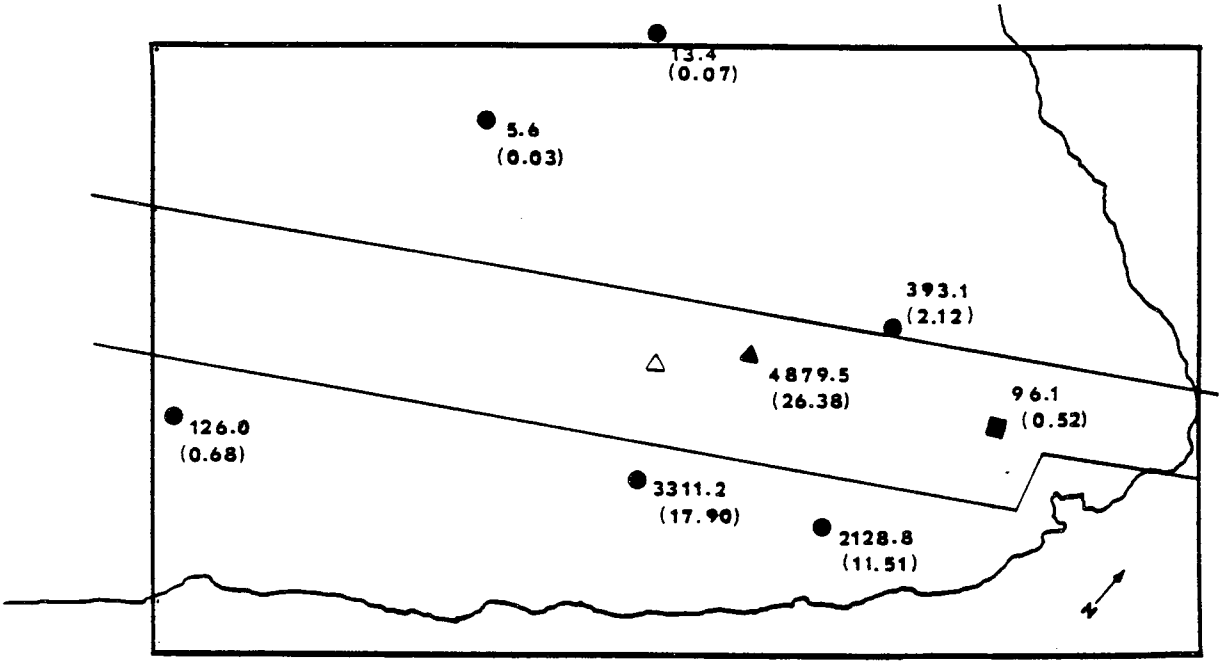

Figure 21b. Changes in Concentration for 1981 in ppm, numbers in () are % salinity of seawater

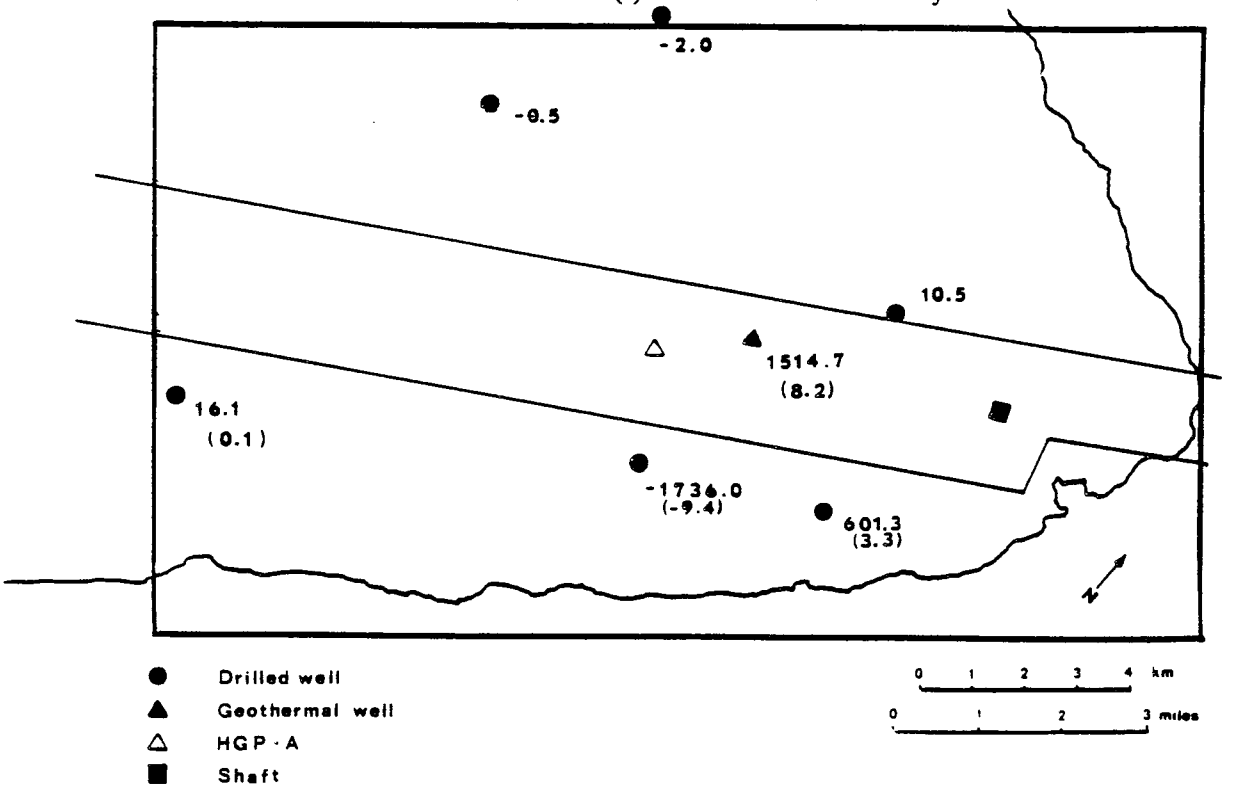

only a couple of years, therefore the system is probably still in a nonsteady state situation. Finally, the model assumes that the injection of the effluent occurs directly into the water table and not as seepage from the ground surface as actually occurs at HGP-A. Thus, actual observed results might be expected to show even less of an increase in salinity because of dilution diffusion and absorption between the ground surface and the water table.

CHAPTER V

SUMMARY OF CONCLUSIONS AND RECOMMENDATIONS

Conclusions

There were two objectives in this study: first, to gain insights into the mechanisms controlling the hydrology of Puna, and second, to examine the effects of effluent disposal on the shallow groundwater. To accomplish this, a numerical model was constructed to simulate the hydrology of Puna.

The calibration of the model aided in the understanding the hydrology of Puna. The east rift zone is a major factor when considering the groundwater flow in Puna. A rift model consisting of two distinct permeabilities gave results which best fit the actual observed well data. In this model, the upper portion of the rift has permeabilities of 9.8×10^{-8} cm^2 (10 darcys) which makes it much more effective as a barrier and causes large head gradients to form. The lower portion of the rift has a much higher permeability, 9.8×10^{-6} cm^2 (1000 darcys), which is nearly as high as the permeability of the non-rift area (4.5×10^{-5} cm^2 or 5000 darcys).

Another major influence on the groundwater flow in the area is heat. High temperature, and therefore, high dynamic viscosities caused estimates for the hydraulic conductivities to be very large. The conductivities ranged between 4337.3 to 8277.1 m/d for the non-rift areas, 17.8 to 32.4 m/d for the upper rift section and 2350.1 to 881.0 m/d for the lower rift section, which is much higher than normally estimated for Hawaiian basalts. The higher temperatures also caused the amount of vertical mixing to increase. The dispersivities were calculated as a function of temperature to incorporate the additional influx of chlorides due to mixing. The dispersivity values ranged

from 501.4 m for temperatures of 22 °C to 4003.9 m for temperatures of 75 °C. The calculated dispersivities were also much larger than normally estimated.

The estimated parameters were then used in the flow submodel to simulate the hydrology of Puna. The velocity values were calculated using the gradients and the hydraulic conductivities. Due to the low hydraulic conductivities assigned to the rift zone, the velocities calculated for the rift were very low, between 0.04 to 3.34 m/d. The calculated velocities of the non-rift areas, however were high ranging from 1.6 to 16.7 m/d north of the rift and 0.7 to 27.7 m/d south of the rift.

A water budget was calculated for the area. The recharge from precipitation was 2.206×10^8 m^3/yr, the discharge from the wells was 2.157×10^4 m^3/yr, and the discharge to the ocean was 2.071×10^8 m^3/yr. This leaves approximately 1.95×10^7 m^3/yr of water unaccounted for. The difference may be due to the anisotropic nature of the rift zone which allows water to flow through the rift or due to some vertical leakage of water to deeper reservoirs such as the geothermal reservoir tapped by HGP-A. Neither of these factors were considered in this model.

Once the model was calibrated, the effects of the seepage of geothermal effluent on the groundwater system could be studied. The simulations showed that the consequences of the injection of geothermal effluent is a direct function of the salinity of the effluent. The seepage of effluent of very high salinities may cause long term water quality problems. The model was further tested by comparing the results of the simulations with chloride concentrations measured from the wells in 1981. The model underestimated the changes in the chloride concentrations. This may be due to several factors:

first the length of the sampling period could not remove the temporal effects of recharge. The system also may not have had enough time for a steady state to be achieved.

A word of caution is in order here. Many assumptions were made in this modeling study. These assumptions limit the accuracy of the modeling results. Some of the major assumptions include: heads, concentrations and other parmeters are vertically averaged, the permeability and dispersivity are considered isotropic, the thicknesses can be calculated using the Ghyen-Herzberg relationship, the solute is nonreactive and the system is assumed to be steady state.

Recommendations

This model was the first attempt to incorporate the effects of groundwater flow, chemistry and temperature in a numerical model for Puna. Recommendations for continued study include:

1. The accuracy of the model is highly dependent on the estimates of the permeabilities used. The model would be greatly improved by allowing the permeabilities to be anisotropic. This would be much more representative of the geology of the area.

2. Reduction of boundary effect would also improve the model. This could be accomplished either by reducing the grid size or allowing the area to be divided into grids of different sizes. This would allow closer examination of specific areas of interest and also reduce the effects of the boundaries.

3. Heat plays a significant role in the hydrology of Puna. Heat was incorporated in this model using the dynamic viscosity. But further

examinations of the effects of heat on dispersion and transport are important. One method would be to consider heat as another variable in the transport submodel.

4. This model assumed that the heads, concentrations, and temperatures did not vary vertically. However, the variations of temperature, concentration, porosity and density are more pronounced in the vertical direction. A better understanding of groundwater flow might be attained if a vertical cross-section were modeled. Also the effects of geothermal activity on the freshwater lens could be examined.

5. For this study, the system was assumed to be steady state. Therefore, the system's response to short-term phenomena such as rainfall was not examined. The nonsteady state conditions may be interesting.

APPENDICIES

APPENDIX

APPENDIX A

Table 6

Summary of Head Data[f]

Date	Heads for the Puna Wells (ft)									
	2487-01 9-7	2487-02	2783-01 9-9	2881-01 A	2982-01 GTW-3	2986-01 9-5A	2986-02 9-5B	3080-02 K	3081-01 9-6	3185-01 9-11
1960						17.66[c]			3.15[c]	
1961	2.94[c]								3.2[e]	
1962			0.56[c]							10.59[c]
			0.86[c]							
1968	3.0[a]		<1.0[a]			18[a]			3[a]	10[a]
1973	3.0[a]		1[b]			18[b]		3[b]	3[b]	10[b]
						17.8[e]				
1974	2.9[e]	3.10[e]	0.9[e]					2.6[e]		10.6[e]
1975				5.0[e]						
Jan			2.2					3.3		
Mar			1.4					2.8		
May			1.5							
Jun			1.2							
Aug			2.3							
Nov			2.0					2.3		
Dec			1.2					3.4		
1976										
Feb			1.5					2.8		
May			1.5					3.6		
Jul			1.0					3.3		
Sept			1.8					3.7		
Nov			1.7					3.6		
Dec			1.7					3.6		

Table 6. (Continued) Summary of Head Data[f]

Date	Heads for the Puna Wells (ft)									
	2487-01 9-7	2487-02	2783-01 9-9	2881-01 A	2982-01 GTW-3	2986-01 9-5A	2986-02 9-5B	3080-02 K	3081-01 9-6	3185-01 9-11
1977										
Mar			1.2					3.1		
May			1.5					3.2		
Jul			3.6					1.7		
Sept			3.2					2.6		
1978										
Jan			1.4					2.5		
Mar			1.5					3.6		
May			1.1					3.4		
Jul			1.3					3.6		
Aug			1.7					2.6		
Oct			2.1					4.0		
Nov			1.9					3.9		
1979										
Jan			1.8					3.8		
Mar			1.9					3.1		
Apr			1.6					4.1		
May			2.0					3.9		
Jul			1.3					3.6		
Sept			1.9					2.5		
1980										
Jan			2.1					2.9		
Mar			1.6					3.7		
May			1.5					3.7		
Sept			2.0					3.3		
Nov			2.0					3.0		
			0.7[d]	4.9[d]	5.2[d]			3.0[d]	3.2[d]	

Table 6. (Continued) Summary of Head Data[f]

	Heads for the Puna Wells (ft)									
	2487-01 9-7	2487-02	2783-01 9-9	2881-01 A	2982-01 GTW-3	2986-01 9-5A	2986-02 9-5B	3080-02 K	3081-01 9-6	3185-01 9-11
Averages	3.0	3.1	1.6	4.95	5.2	17.9		3.2	3.1	10.3
S. D.	0.05		0.59	0.07		0.12		0.56	0.10	0.34
# samples	4	1	41	2	1	3		34	5	4
head (m)	0.9	0.9	0.5	1.5	1.6	5.5		0.98	0.9	3.1

a. Davis and Yamanaga, 1968
b. Davis and Yamanaga, 1973
c. DOWALD, 1970
d. Epp and Halunen, 1979
e. Thomas et al., 1979
f. USGS Site Inventory Data

APPENDIX B

Table 7

Summary of Temperature Data[i]

Date	Temperatures for the Puna Wells (C)									
	2487-01 9-7	2487-02	2783-01 9-9	2881-01 A	2982-01 GTW-3	2986-01 9-5A	2986-02 9-5B	3080-02 K	3081-01 9-6	3185-01 9-11
1960									33.9[c]	
1961	23.3[c]					22.2[c]			28.0[h]	
1962			53.9[b]							
1964										21.7[c]
1972										
Mar	23.0[g]					22.5[g]	22.5[g]			
1973						22.5[h]				
Mar						22.0	22.5			
May						22.0				
Jul							22.0	25.0		
Aug										21.0
Sept										21.5
Oct										22.0
Nov										21.8
1974	24.0[h]	24.0[h]	53.0[h]				23.0[h]	25.0[h]		21.5[h]
Jan	23.3[d]	23.5	54.0	38.0		22.2[d]		25.0	38.0[a]	22.0
Mar						22.0	22.0			
Apr										21.0
May										22.0
Jun			56.0							
Aug			52.8[e]	37.8[e]	92.1[e]				32.8[e]	
Sept							22.5	25.0		22.0
Dec					86.0[a]				34.0[a]	21.5

Table 7. (Continued) Summary of Temperature Data[i]

Date	Temperatures for the Puna Wells (C)									
	2487-01 9-7	2487-02	2783-01 9-9	2881-01 A	2982-01 GTW-3	2986-01 9-5A	2986-02 9-5B	3080-02 K	3081-01 9-6	3185-01 9-11
1975				37.5[h]						
Jan	28.5[f]		52.2[a]	37.8[a]	93.0[a]			25.5[f]	36.8[f]	
Feb										21.0
Mar						22.0	22.0			
May										22.0
June								25.0		
July	20.8[f]					23.0[f]		22.1[f]	38.5[a]	22.0
Sept			53.6[e]		92.5[e]				36.0[e]	
			52.5							22.0
Nov			53.5					25.5		22.0
Dec			53.0							
1976										
Jan			51.4[e]		91.7[e]				34.3[e]	
										21.5
Feb	23.5		54.0					25.0		
May			53.0							21.0
July			54.0							21.0
Sept										21.5
Oct			55.0							
Nov			54.5							21.5
Dec			55.0			22.5	22.5			
1977										
Mar			55.0							21.5
May			52.0							21.5
July			54.0					25.0		
Sept	24.0		53.0			22.5	22.5	25.0		

Table 7. (Continued) Summary of Temperature Data[i]

Date	Temperatures for the Puna Wells (C) 2487-01 9-7	2487-02	2783-01 9-9	2881-01 A	2982-01 GTW-3	2986-01 9-5A	2986-02 9-5B	3080-02 K	3081-01 9-6	3185-01 9-11
1978										
Jan			54.0					25.0		
Mar			55.0			22.5	22.5			
May			54.0			22.5	22.5			
Aug			54.0			22.5	22.5	25.5		21.0
Oct			54.0							21.0
Nov			54.0							
1979										
Jan			52.0							
Mar			52.0			22.0	22.0	25.0		
Apr			51.0			22.0	22.0			
May			52.0							
Jun										21.0
Jul			54.0							21.0
Sept			54.0			22.5	22.5	25.0		
1980										
Jan			54.0							
Mar			54.0							
May			53.5							
Sept			53.5			22.5	22.5	25.5		21.0
Nov			53.0			23.0	23.0	25.5		
Averages	23.8	23.5	53.5	37.8	91.1	22.4	22.4	25.0	34.2	21.5
S. D.	2.2	0.4	1.1	0.2	2.9	0.3	0.3	0.8	2.9	0.4
# samples	8	2	39	4	5	19	16	17	9	28

a. Cox and Thomas, 1979
b. DOWALD, 1962
c. DOWALD, 1970
d. Druecker and Fan, 1976
e. Epp and Halunen, 1979
f. Kroopnick et al., 1978
g. Swain, 1973
h. Thomas et al., 1979
i. USGS Site Inventory Data

APPENDIX C

Table 8

Summary of Chloride Data[i]

Date	Chloride Concentrations for the Puna Wells (mg/l)									
	2487-01 9-7	2487-02	2783-01 9-9	2881-01 A	2982-01 GIW-3	2986-01 9-5A	2986-02 9-5B	3080-02 K	3081-01 9-6	3185-01 9-11
1960						2[c]			338[c]	
1961	74[c]								331[a]	
									220[h]	
1962			5820[g]	6200[c]						
1964										16[c]
1968	90[b]		7000[b]			6[b]		125[g]	350[b]	16[b]
1970								72[g]		
1972										23[g]
Mar	70[g]					6[g]		54[g]		
1973						12.0[h]				
Mar		110				4.0	5.0	100		
May		110				5.0		110		
Jul		110	6500			6.0	6.0	120		
Aug										14
Sept			6600							14
Oct			6500							14
Nov			6500							15
1974	70[h]	160[h]	5850[h]	1400[a]			5.8[h]	170[h]	338[d]	14[h]
										28[h]
Jan	82[d]	120	4600	722[d]		2[d]		130	560[a]	14
			11000[a]					180[d]		
Mar			5500				7.0			
Apr										15
May			4500							14
Jun			4600							

Table 8. (Continued) Summary of Chloride Data[i]

Date	Chloride Concentrations for the Puna Wells (mg/l)									
	2487-01 9-7	2487-02	2783-01 9-9	2881-01 A	2982-01 GTW-3	2986-01 9-5A	2986-02 9-5B	3080-02 K	3081-01 9-6	3185-01 9-11
Aug			5200							14
			6200[d]							
Sept					2000[d]					
Nov			5200				7.0	110		
Dec			11000[a]		4200[a]				750[a]	14
1975				281[h]	3410[h]					
			3850[a]							
Jan	132.2[e]		2100		3274[e]	13.5[e]			303.5[e]	
			3811[e]	281[a]						
Feb										15
Mar			3400			6.0	6.0			
May			4000							14
June			4700					90		
July	120.0[e]		5120[e]		3410[e]	9.8[e]		95.7[e]	316[e]	16
Aug			5200							
Sept										16
Oct								105[a]		
Nov			5800					110		16
Dec			4500							
1976										
Jan										16
Feb		120	3200					100		16
May			4800							14
July			6100					150		12
Sept								170		11
Oct			5900							
Nov			5800							15
Dec			5800			5.0	5.0			

Table 8. (Continued) Summary of Chloride Data[i]

Date	Chloride Concentrations for the Puna Wells (mg/l)									
	2487-01 9-7	2487-02	2783-01 9-9	2881-01 A	2982-01 GTW-3	2986-01 9-5A	2986-02 9-5B	3080-02 K	3081-01 9-6	3185-01 9-11
1977										
Mar			5900							16
May			2500							14
July			5000					150		
Sept		160	5000			5.5	5.5	170		
1978	70[a]	160[a]	5850[a]	281[a]	3410[a]	12[a]		170[a]	320[a]	14[a]
Jan			2800					210		
Mar			5500			5.5	5.5			
May			5400			6.0	6.0			
July			5500							
Aug			5000			6.0	6.0	170		16
Oct			4900							18
Nov			4100							
1979										
Jan			2400							
Mar			2100			6.0	6.0	90		
Apr			2300			5.5	5.5			
June										15
July			4300							14
Sept			4800			6.0	6.0	150		
1980										
Jan			4900							
Mar			4800							
May			4200							
Sept			4900			4.5	4.5	140		15
Nov			4400			6.0	6.0	180		

Table 8. (Continued) Summary of Chloride Data[i]

Date	Chloride Concentrations for the Puna Wells (mg/1)									
	2487-01 9-7	2487-02	2783-01 9-9	2881-01 A	2982-01 GTW-3	2986-01 9-5A	2986-02 9-5B	3080-02 K	3081-01 9-6	3185-01 9-11
Averages	88.5	131.3	5047.2	1527.5	3364.9	6.4	5.8	132.6	382.7	15.4
S. D.	24.4	24.2	1689.7	2330.6	684.4	2.9	0.7	38.9	154.6	3.0
# samples	8	8	54	6	7	23	16	28	10	32
% salinity	0.47	0.7	27.2	8.3	18.2	0.03	0.03	0.7	2.1	0.08

a. Cox and Thomas, 1979
b. Davis and Yamanaga, 1968
c. DOWALD, 1970
d. Druecker and Fan, 1976
e. Kroopnick et al., 1978
f. McMurtry et al., 1977
g. Swain, 1973
h. Thomas et al., 1979
i. USGS Site Inventory Data

APPENDIX D

Table 9

Summary of Silica Data

Date	Silica Concentrations for the Puna Wells (mg/l)									
	2487-01 9-7	2487-02	2783-01 9-9	2881-01 A	2982-01 GTW-3	2986-01 9-5A	2986-02 9-5B	3080-02 K	3081-01 9-6	3185-01 9-11
1960						30.4[b]				
1961	44.0[b]							70.5[b]		
1962			59[b]							
1964										58.8[b]
1968									44[f]	49[f]
1970									39[f]	
1972										
Mar	41.0[f]					54.0[f]	50[f]		39[f]	
1973						39.6[g]				
1974	41.0[g]	45.3[g]	59.0[g]				55[g]	58[a]	70.5[a]	51.9[g]
Jan	48[e]		90[e]	53[e]			60[e]	56[e]	56[e]	49[g]
Sept					178[e]					
Dec					184[e]				53[e]	
					187[a]					
1975										
Jan	44.5[d]		100.7[d]	24.1[d]	96.6[d]	50[d]		53.6[d]	71.3[d]	
			50[c]		179[c]					
			50[c]		189[c]					

Table 9. (Continued) Summary of Silica Data

Date	Silica Concentrations for the Puna Wells (mg/l)									
	2487-01 9-7	2487-02	2783-01 9-9	2881-01 A	2982-01 GTW-3	2986-01 9-5A	2986-02 9-5B	3080-02 K	3081-01 9-6	3185-01 9-11
Averages	43.7	45.3	68.1	38.6	168.9	47.9	55.0	59.5	53.3	52.2
S. D.	2.9		21.7	20.4	35.7	7.4	5.0	7.5	13.7	4.6
# samples	5	1	6	2	6	3	3	4	7	4

a. Cox and Thomas, 1979
b. DOWALD, 1970
c. Druecker and Fan, 1976
d. Kroopnick et al., 1978
e. McMurtry et al., 1977
f. Swain, 1973
g. Thomas et al., 1979

REFERENCES CITED

Bachmat, Y., J. Bredehoeft, B. Andrews, D. Holz, S. Sebastian. 1980. Groundwater management: the use of numerical models. American Geophysical Union, Water Resources Monograph 5, 127 pp.

Bear, J. 1972. Dynamics of fluid in porous media. American Elsevier Publishing Co., New York, 764 pp.

Bear, J. 1979. Hydraulics of groundwater. Mcgraw-Hill, New York, 569 pp.

Breddia, C. A. 1978. The boundary element method for engineers. John Wiley and Sons, New York, 189 pp.

Bredehoeft, J. D. and G. F. Pinder. 1970. Digital analysis of areal flow in multiaquifer groundwater systems: a quasi three-dimensional model. Water Resources Research, vol. 6, no. 3, pp. 883-888.

Bredehoeft, J. D. and G. F. Pinder. 1973. Mass transport in flowing groundwater. Water Resources Research, vol. 9, no. 1, pp. 194-210.

Broyles, M. L., W. Suyenaga, and A. S. Furumoto. 1979. Structure of the lower east rift zone of Kilauea Volcano, Hawaii, from seismic and gravity data. Journal of Volcanology and Geothermal Research, vol. 5, pp. 317-336.

Buddemier, R., P. Kroopnick, and L. S. Lau. 1976. Progress report: hydrology. In: Initial Phase II Progress Report, The Hawaii Geothermal Project, pp. 45-50.

Carnahan, B., H. A. Luther, and J. O. Wilkes. 1969. Applied numerical methods. John Wiley and Sons, New York, 604 pp.

Cheng, P. and K. H. Lau. 1978. Modeling of a volcanic island reservoir. The Hawaii Geothermal Project, 39 pp.

Cox, M. E. and D. M. Thomas. 1979. Chloride/magnesium ratio of shallow groundwaters as a regional geothermal indicator in Hawaii. Hawaii Institue of Geophysics Technical Report, HIG 79-9, 51 pp.

Dagan, G. and J. Bear. 1968. Solving the problem of local interface upconing in a coastal aquifer by the method of small perturbations. Journal of Hydraulic Research, vol. 6, no. 1, pp. 15-44.

Das Gupta, A., and P. N. D. D. Yapa. 1982. Saltwater enchroachment in an aquifer: a case study. Water Resources Research, vol. 18, no. 3, pp. 546-556.

Davis, D. A. and G. Yamanaga. 1968. Preliminary reports on the water resources of the Hilo-Puna area, Hawaii. Hawaii Division of Water and Land Development Circular C45, 38 pp.

Davis D. A. and G. Yamanaga. 1973. Water resources summary, Island of Hawaii. U. S. Geological Survey Report, R47, 42 pp.

Department of Land and Natural Resources, Division of Water and Land Development, State of Hawaii. 1962. Summary of drilling logs and pumping test for Malama-ki well 9-9, Puna Hawaii. Circular C12, 11 pp.

Department of Land and Natural Resources, Division of Water and Land Development, State of Hawaii. 1964. Summary of drilling and pumping test for Pulama well 9-10, Pulama, Puna, Hawaii. Circular C26, 12 pp.

Department of Land and Natural Resources, Division of Water and Land Development, State of Hawaii. 1970. An investigation of basic water resources data, Island of Hawaii. Report, R34, 188 pp.

Department of Land and Natural Resources, Division of Water and Land Development, State of Hawaii. 1982. Median rainfall, State of Hawaii. Circular C88.

Department of Water Supply, County of Hawaii. 1971-1981. Big Island Well and Pumpage reports.

Druecker, M. and P. F. Fan. 1976. Hydrology and chemistry of groundwater in Puna, Hawaii. Ground Water, vol. 14, no. 5, pp. 339-350.

Epp, D., R. W. Decker, and A. T. Okamura. 1983. Relation of summit deformation to East Rift Zone eruptions on Kilauea Volcano, Hawaii. Geophysical Research Letters, vol. 10, no. 7, pp. 493-496.

Epp, D. and H. J. Halunen Jr. 1979. Temperature profiles in well on the Island of Hawaii. Hawaii Institute of Geophysics Technical Report, HIG 79-7. 31 pp.

Eyre, P. 1977. A hydrologic study of an area around the Hawaii Geothermal Project well HGP-A. Unpublished report.

Faust, C. R., J. W. Mercer. 1980. Ground-water modeling: numerical models. Ground Water, vol. 18, no. 4, pp. 395-409.

Fischer, W. A., R. M. Moxham, F. Polcyn, G. H. Landis. 1964. Infrared surveys of Hawaiian volcanoes. Science, vol. 146, pp. 733-742.

Freeze, R. A. and J. A. Cherry. 1979. Groundwater. Prentice-Hall Inc., Englewood Cliffs, N. J., 604 pp.

Fried, J. J. 1975. Groundwater pollution. Elsevier Scientific Publishing Co., Amsterdam, 330 pp.

Furumoto, A. S., G. A. Macdonald, M. Druecker, and P. F. Fan. 1977. Preliminary studies for geothermal exploration in Hawaii, 1973-1975. Hawaii Institute of Geophysics Technical Report, HIG 75-5, 55 pp.

Holcomb, R. T. 1980. Preliminary geologic map of Kilauea Volcano, Hawaii. U. S. Geologic Survey Open File Report 80-796

Hubbert, M. K. 1940. The theory of ground-water motion. The Journal of Geology, vol. 48, no. 8, pp. 785-944.

Imada, J. A. 1982. Investigation of the geohydrology of Puna, Hawaii. Unpublished report, 43 pp.

Kanehiro, B. Y. and F. L. Peterson. 1977. Groundwater recharge and coastal discharge for the northwest coast of the Island of Hawaii: a computeried water budget approach. Water Resources Research Center Technical Report No. 110, 83 pp.

Keller, G., C. K. Skokan, J. J. Skokan, J. Daniels, J. P. Kauahikaua, D. P. Klein, C. J. Zablocki. 1977. Geoelectric studies on the East Rift, Kilauea Volcano, Hawaii Island. Hawaii Institute of Geophysics Technical Report, HIG 77-15, 195 pp.

Kemblowski, M. 1983. Simulation of fresh-water-salt-water interface movement by boundary element method. EOS, Transactions, American Geophysical Union, vol. 64, no. 18, pg. 225.

Klein, D. P. and J. P. Kauahikaua. 1975. Geoelectric-geothermal exploration on Hawaii Island: preliminary results. Hawaii Institute of Geophysics Technical Report, HIG 75-6, 23 pp.

Konikow, L. F. and J. D. Bredehoeft. 1974. Modeling flow and chemical quality changes in an irrigated stream-aquifer system. Water Resources Research, vol. 10, no. 3, pp. 546-562

Konikow, L. F. and J. D. Bredehoeft. 1978. Computer model of two-dimensional solute transport and dispersion in ground water. Techniques of Water-Resources Investigations of the U. S. Geological Survey, Book 7, Chapter C2, 90 pp.

Kroopnick, P. M., R. W. Buddemier, D. Thomas, L. S. Lau,and D. Bills. 1978. Hydrology and geochemistry of a Hawaii geothermal system: HGP-A. Hawaii Institute of Geophysics Technical Report, HIG 78-6, 64 pp.

Kroopnick, P. M., D. Thomas, L. S. Lau, R.W. Buddemier, and D. Bills. 1980. Geochemical techiniques in geothermal research- the Hawaii example. Tectonophysics, v. 62, pp 87-97.

Liu, C. C. K., L. S. Lau, and J. F. Mink. 1981. Numerical simulatio of a thick freshwater lens: Pearl Harbor groundwater model. Groundwater, vol. 21, no. 3, pp. 293-300.

Liu, C. C. K., R. H. Dale and C. J. Ewart. 1984. Ground-water flow and salinity transport in the Beretania basal-water body, island of Oahu, Hawaii. U. S. Geological Survey Water-Resources Investigation Report.

Macdonald, G. A. 1977. Geologic conditions. In: Reservior Assessment for HGP-A, Hawaii Geothermal Project Report, pp. 1-8

Macdonald, G. A., A. T. Abbot, and F. L. Peterson. 1983. Volcanoes in the sea the geology of Hawaii. Unversity of Hawaii Press, Honolulu, Hi., 517 pp.

McMurtry G. M., P. F. Fan, and T. B. Coplen. 1977. Chemical and isotopic investigations of groundwater in potential geothermal areas in Hawaii. American Journal of Science, vol. 277, pp 438-458.

Mercer, J. W., S. P. Larson, and C. R. Faust. 1980. Simulation of salt-water interface motion. Ground Water, vol. 18, no. 4, pp. 374-385.

Palmiter, D. B. 1976. Geology of HGP-A from macroscopic study of cores and cuttings. Unpublished report.

Pinder, G. F. and J. D. Bredehoeft. 1968. Application of the digital computer for aquifer evaluation. Water Resources Research, vol. 4, no. 5, pp. 1069-1093.

Pinder, G. F. and H. H. Cooper Jr. 1970. A numerical technique for calculating the transient position of the seawater front. Water Resources Research, vol. 6, no. 3, pp 875-882.

Pinder, G. F. and W. G. Gray. 1977. Finite elemment silmulation in surface and subsurface hydrology. Academic Press, New York, 295 pp.

Polo, J. F. and F. J. R. Ramis. 1983. Simulation of salt water-fresh water interface motion. Water Resources Research, vol. 19, no. 1, pp. 61-68.

Redell, D. L. and D. K. Sunada. 1970. Numerical simulation of dispersion in groundwater aquifers. Colorado State University, Hydrology Paper No. 41, 79 pp.

Remson, I., G. M. Hornberger, and F. J. Molz. 1971. Numerical methods in subsurface hydrology. Wiley-Interscience, New York, 389 pp.

Scheidegger, A. E. 1961. General theory of dispersion in porous media. Journal of Geophysical Research, vol. 66, no. 10, pp. 3273-3278

Shamir, V. and G. Dagan. 1971. Motion of the seawater interface in coastal aquifers: a numerical solution. Water Resources Research, vol. 7, no. 3, pp 644-657.

Stearns, H. T. and G. A. Macdonald. 1946. Geology and ground-water resources of the Island of Hawaii. Hawaii Hydrography Division Bulletin No. 9, 363 pp.

Stone, C. 1977. Geochemistry. In: Progress Report for the Third Quarter of Federal Fiscal Year 1977; Phase III, Well Testing and Analyses. Hawaii Geothermal Project.

Suyenaga, W., M. Broyles, A. S. Furumoto, R. Norris, and M. D. Mattice. 1978. Seismic studies on Kilauea Volcano, Hawaii Island. Hawaii Institute of Geophysics Technical Report, HIG 78-8, 137 pp.

Swain, L. A. 1973. Chemical quality of ground water in Hawaii. Department of Land and Natural Resources, Division of Water and Land Development, State of Hawaii, Report r48, 54 pp.

Takasaki, K. J. 1978. Summary appraisals of the nation's ground-water resources: Hawaii region. U. S. Geological Survey Proffessional Paper 813-m, 29 pp.

Thomas D. M., M. Cox, D. Erlandson, and L. Kajiwara. 1979. Potential geothermal resources in Hawaii: a preliminary survey. Hawaii Institute of Geophysics Technical Report, HIG 79-4, 103 pp.

Thomas, D. M. and H. Sakai. 1983. Chemical and isotopic studies of the HGP-A geothermal well. Extended Abstracts, Fourth Annual International Symposium of Water-Rock Interactions, pp 479-482

Trescott, P. C., G. F. Pinder and S. P. Larson. 1976. Finite-difference model for aquifer simulation in two dimensions with results of numerical experiments. Techniques of Water-Resources Investigations of the U. S. Geological Survey, Book 7, Chapter C1, 116 pp.

Wang, H. F. and M. P. Anderson. 1982. Introduction to groundwater modeling. W. H. Freeman and Co., San Francisco, 237 pp.

Weast, R. C., ed. 1972. Handbook of chemistry and physics. Cleveland, Ohio, The Chemical Rubber Company.

Wheatcraft, S. W. and F. L. Peterson. 1979. Numerical modeling of liquid water injection into a two-phase fluid system. Water Resources Research Center Technical Report No. 125, 103 pp.

Williams, J. A. and R. L. Soroos. 1973. Evaluation of methods of pump test analysis for application to Hawaiian aquifers. Water Resources Research Center Technical Report No. 70, 159 pp.

Yuen, P. C., B. H. Chen, D. H. Kihara, A. S. Seki, P. K. Takahashi. 1978. HGP-A reservior engineering. Hawaii Geothermal Project Progress Report, 96 pp.